Tensile Strength Enhancement of Fused Filament Fabrication Printed Parts: A Review of Process Improvement Approaches and Respective Impact

Author

Tran, Thang Q, Ng, Feng Lin, Kai, Justin Tan Yu, Feih, Stefanie, Nai, Mui Ling Sharon

Published

2022

Journal Title

Additive Manufacturing

Version

Accepted Manuscript (AM)

DOI

10.1016/j.addma.2022.102724

Tensile Strength Enhancement of Fused Filament Fabrication Printed Parts: A Review of Process Improvement Approaches and Respective Impact

Thang Q. Tran, Feng Lin Ng, Justin Tan Yu Kai, Stefanie Feih, Mui Ling Sharon Nai*

Singapore Institute of Manufacturing Technology, 73 Nanyang Drive, 637662, Singapore

Published as: Additive Manufacturing, 54: 102724, June 2022

DOI: 10.1016/J.ADDMA.2022.102724

Corresponding author: mlnai@simtech.a-star.edu.sg (M.L.S.N)

Abstract:

Fused Filament Fabrication (FFF) is a rapidly growing and widely used 3D printing process with many practical applications thanks to its superior advantages such as ease of handling, cost-efficiency, and ability to fabricate complex structures with reduced waste and shorter production time. However, the mechanical property deficiency and related anisotropy with respect to build direction of FFF printed parts is still one of the most crucial challenges due to inherent process limitations and material properties, resulting in internal defects in printed structures. This review article offers researchers and users in the FFF community guidance to evaluate and determine impactful methods for manufacturing polymer printed parts with required mechanical strength for a wide range of end-use applications. The paper categorizes, evaluates, and compares a large number of recent publications presenting tensile property improvements of FFF printed parts in longitudinal and transverse directions covering material development, post-treatment, and process modification. Moreover, reported tensile test results are normalised via a calculated improvement efficiency index, and fundamental mechanisms responsible for strength improvements are highlighted. The advantages of and remaining concerns for the respective approaches are then discussed and compared via their respective improvement efficiency indices, thereby highlighting the impact of the proposed evaluation approach.

Keywords: Additive manufacturing; fused filament fabrication; fused deposition modelling; mechanical properties; improvement efficiency index.

1. Introduction

Additive manufacturing (AM), also known as 3D printing, has developed rapidly in recent years and has become one of the key manufacturing technologies in Industry 4.0 [1, 2]. Unlike conventional subtractive manufacturing techniques, which fabricate final parts by removing material, AM is generally based on an additive process where physical objects are built up by adding material gradually one cross-sectional layer at a time directly from their digital model data [2]. Due to the layer-by-layer manufacturing approaches, AM methods can fabricate a wide range of prototypes or functional parts with several advantages, such as the possibility to build complex geometries at lower cost, with less waste material, a shorter lead time, and less assembly requirements [1, 2]. AM technologies can process different materials such as metals, polymers, ceramics, and their composites or hybrids [2], which in turn enables the resulting products to be used in many applications such as aerospace [3, 4], medical and dental applications [5-7], machinery [8], electronics [9-13], automobiles [14], food [15], textile [16-19], construction [20-23], and architecture [24, 25].

Among the wide range of AM-processable materials, polymers play an important role for 3D printing of plastics, polymer matrix composites, and functionally graded materials thanks to their relatively low curing and melting temperatures, good flowability when softened or melted, and high chemical stability [2, 7, 26]. Their feedstock forms for 3D printing processes can be powders, pellets, filaments, sheets, or liquids. Some common AM processes for manufacturing polymeric products are (1) fused filament fabrication (FFF) with polymeric filaments, (2) digital light processing and stereolithography with photopolymer resins, (3) selective laser sintering with polymeric powders, and (4) laminated objective manufacturing with polymeric sheets [2, 26]. Among those manufacturing methods, FFF is one of the most commonly used techniques in both public and industries due to its simple

fabrication process, cost-effectiveness, economic accessibility, reliability, ability to print complex shapes safely in favourable environment, and wide material customization [27].

Despite the widespread use of FFF, one of the main disadvantages is the lower strength of the printed products compared to those produced by traditional manufacturing methods such as conventional plastic extrusion [28, 29]. Owing to the layer-by-layer deposition of polymeric material in the FFF process, the extruded melt material cools down rapidly when it is deposited on the underlying cold layers. Consequently, complete interfacial diffusion between neighbouring filaments and layer bonding through-the-thickness is generally not achieved, leading to the formation of voids and interfaces inside the 3D printed parts. These defects lower the mechanical performance of the FFF printed components compared to the base material properties, hence often limiting the practical applications to prototyping rather than fully functional parts [28-30].

Over the last decade, significant research efforts have focussed on improving the mechanical performance of FFF printed parts so that they can move beyond their initial role as conceptual prototypes to end-use components [28, 29]. Most research studies have focused on optimization of process parameters for high-performance printed parts [31-40], while other new process improvement approaches such as development of new material systems [31, 41-45], application of post-treatments [28, 46-48], and modification of conventional FFF fabrication processes [29, 49, 50] also show improved efficiency. Although several review papers have been published on mechanical properties of FFF printed parts, especially focussing on process parameter optimization studies [31, 32, 51], a comprehensive review focussed on categorizing process improvement approaches for enhancing the mechanical performance and related property anisotropy has yet to be reported. Recent accelerated developments in studies of FFF process innovation have motivated this review.

Tensile properties are the main focus of the review paper as a large volume of pertinent literature on process improvement approaches for strength enhancement is available. Studies on process improvement approaches presented in literature were categorized, evaluated and compared in terms of efficiency. Additionally, for each category, fundamental mechanisms related to the improvement efficiency are summarized based on selected relevant research papers chosen as being representative of the large volume of studies. The review is structured as follows. In Section 2, common materials used in FFF process and the effects of process parameter variation and optimization on the mechanical properties of the printed parts are recapped. Material modification studies and underlying fundamental mechanisms for improving the mechanical strength of FFF printed parts are highlighted and discussed in Section 3. In Section 4, the potential of post-processing methods and their impact on the mechanical properties of FFF-printed parts are discussed. Section 5 then outlines equipment modification research and relates the findings to the fundamental mechanisms explained in the earlier two sections. Conclusions and an outlook for future FFF process development are given in Section 6.

2. FFF printing process

In this section, the fundamental features of the FFF process such as commonly used feedstock materials as well as crucial process parameters and their effects on tensile strength of the FFF printed parts are highlighted. This will help the readers to gain an advanced understanding of the underlying mechanisms resulting in property advancements as presented in Sections 3, 4, and 5.

2.1 Commonly-used materials in FFF processing

Fig. 1a illustrates a typical fabrication process of a 3D part via FFF technique. To build an object, a solid thermoplastic filament is unwound from a filament spool and fed through a heated extruder of a certain diameter [27, 32, 51]. The filament is then heated to its flowing temperature prior to being extruded through a nozzle for material deposition. As the nozzle travels horizontally based on the digital model data of the fabricated part, the extruded melt material is deposited on a printing bed, solidifies rapidly, and adheres with the print bed (first layer) and/or surrounding material (subsequent layers) to produce each layer of the printed part. The printing bed is sometimes heated or conditioned with adhesives to create improved adhesion with the melt material. Some FFF printers are equipped with a heated chamber to minimize the thermal gradient in the printing process. After the built of the corresponding layer is completed, the nozzle or the printing bed moves vertically to a pre-defined layer height, followed by the deposition of the next layer onto the previous one. This layer-by-layer process continues until the required part is fully built [27, 32, 51, 52].

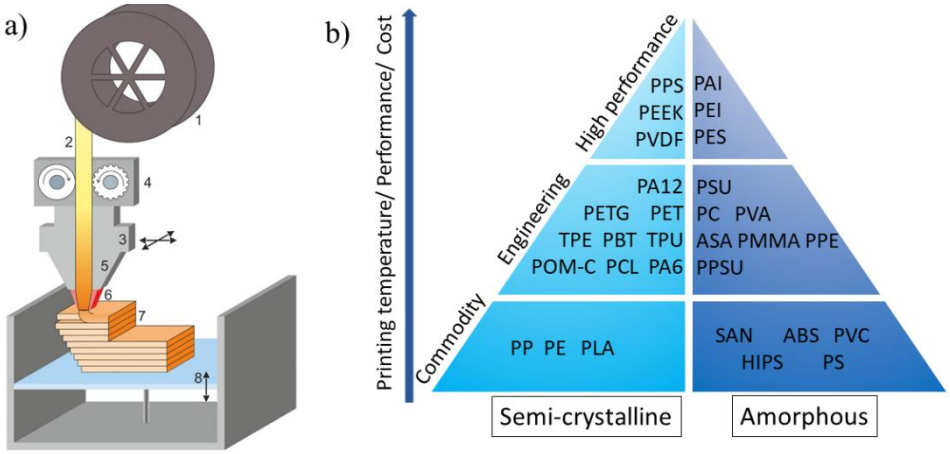

Fig. 1. (a) Schematic illustration of a typical FFF process. The components are labelled as: (1) spooled material storage, (2) thermoplastic filament, (3) horizontally movable, heated deposition unit consisting of (4) counter-rotating driving wheels, (5) a liquefier, (6) a nozzle, (7) structural element fabricated in a layer-by-layer manner, and (8) vertically movable build

platform. (b) A pyramid of thermoplastic materials available in FFF. Reprinted with permission from Ref. [53].

Table 1. Polymer abbreviations in Fig. 1b

Polymer abbreviation			
PPS	Polyphenylene sulfide	**PEEK**	Polyether ether ketone
PVDF	Polyvinylidene fluoride	**PAI**	Polyamide-imide
PEI	Polyethylenimine	**PES**	Polyethersulfone
PA12	Polyamide 12	**PETG**	Polyethylene terephthalate glycol
PET	Polyethylene terephthalate	**TPE**	Thermoplastic elastomers
PBT	Polybutylene terephthalate	**TPU**	Thermoplastic polyurethane
POM-C	Nylacast polyacetal	**PCL**	Polycaprolactone
PA6	Polyamide 6	**PSU**	Polysulfone
PC	Polycarbonate	**PVA**	Polyvinyl alcohol
ASA	Acrylonitrile styrene acrylate	**PMMA**	Poly(methyl methacrylate)
PPE	Polyphenylene ether	**PPSU**	Polyphenylsulfone
PP	Polypropylene	**PE**	Polyethylene
PLA	Polylactic acid	**SAN**	Styrene acrylonitrile
ABS	Acrylonitrile butadiene styrene	**PVC**	Polyvinyl chloride
HIPS	High impact polystyrene	**PS**	Polystyrene

One key strength of the FFF technique is its wide range of available materials used for printing [21, 31, 32, 52, 53]. Fig. 1b shows a pyramid of common thermoplastic materials available for the FFF printing process. Table 1 provides a full list of the abbreviations of the various thermoplastic materials. Generally, materials located at a higher position in the pyramid achieve superior mechanical properties, but also require higher printing temperature and therefore have an increased processing cost. Polymeric thermoplastic materials used in

the FFF process can be classified into two different types: semi-crystalline and amorphous polymers. The presence of crystalline and amorphous phases in a polymer affects the processability of the material in an extrusion-based system significantly [52, 53]. Due to the arrangement of crystallites in the crystalline phase, semi-crystalline polymers experience drastic changes in specific volume during cooling, leading to significantly higher shrinkage compared to amorphous polymers, and the resulting fabricated parts are prone to shrinkage, warpage, and distortion [52-55]. Therefore, it is more challenging to process semi-crystalline polymers via FFF processing compared to amorphous materials, especially for those with a high degree of crystallinity (>40%). Although the issues of shrinkage, warpage, and distortion are less severe during 3D printing of amorphous polymers, their performance related to mechanical loading, chemical resistance, and service temperature limits is generally lower than that of semi-crystalline polymers [52, 53].

Based on the polymer grade, the materials used in FFF processing can also be divided into 3 main groups: commodity, engineering, and high-performance polymers [53]. The commodity polymers are usually used for general purpose applications such as prototyping, concept models, and end-use parts with low static loading. The engineering polymers with medium performance are suitable for engineering applications such as functional parts with low volume production and high customization as well as machine tools. Due to their much higher mechanical and physical properties, the high-performance polymers are used in high-end engineering applications such as aerospace and automotive. Notably, both engineering and high-performance polymers are attractive to many industrial applications due to their high thermal and chemical resistances to many harsh environments, high strength-to-weight ratios and other advantages over some metals. However, a proper heat management system is usually required for FFF printing of these polymers to prevent print failure [56]. Up to now, PLA and ABS are the most widely used materials in FFF processing thanks to their facile

processability with low distortions or warpage [32-34, 51, 53]. However, recently more niche materials have been under investigation and several new materials are available for the use in the FFF process, indicating a rapid growth in the material variety for this printing technology [31].

2.2 Printing parameters and their effects on mechanical strength of FFF printed parts

Fig. 2 presents a configuration of a printing layer and the build orientation in FFF processing. Important processing parameters such as build orientation, layer thickness, infill density, raster angle, air gap, contour width, and number of contours have all been correlated with the tensile strength of FFF printed parts [35-37, 57-61].

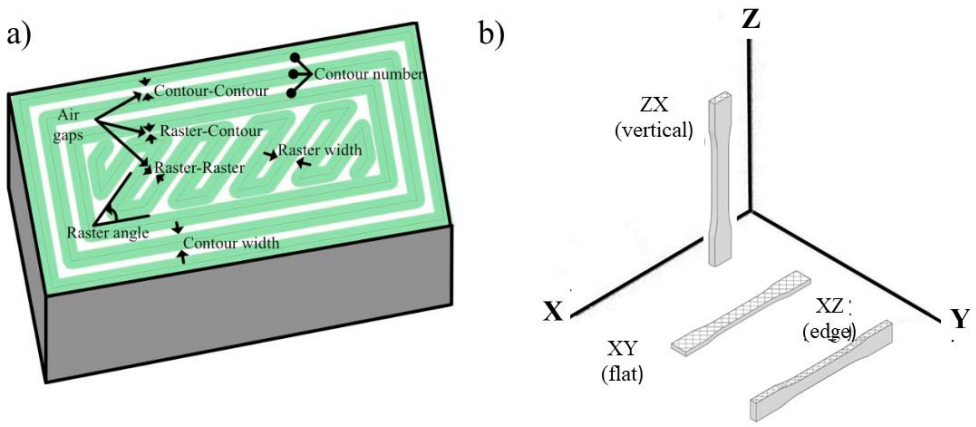

Fig. 2. Schematic illustration of (a) a single layer configuration and (b) build orientation printed via FFF processing. Reprinted with permission from Ref. [62]

2.2.1 Contour number

Contour refers to the outer shells of the part built by FFF processing to form the part shape prior to filling the interior. Due to its concentric deposition around the printed part, the contour is usually aligned with load direction and independent of infill raster angle. Therefore, a larger number of contours can increase the deposited material in the load direction for higher load-bearing ability, resulting in improved tensile strength and Young's modulus [62-65]. The positive effects of high contour number on the tensile performance of

FFF printed parts have been reported in several research studies [62-65]. For instance, the study of Croccolo *et al.* suggested that tensile strength and Young's modulus of the printed ABS parts increased by 24% and 17%, respectively, when increasing the contour number from 1 to 10 [63].

2.2.2 Layer thickness

Layer thickness is the height of the polymeric layer deposited along the Z-axis. It has been reported that the layer thickness has a crucial effect on the tensile properties of the FFF printed parts. Specifically, 3D parts printed at a smaller layer thickness have improved inter-layer strength [57-59]. As the gap between the printer nozzle and the printed part surface is reduced when printing with a smaller layer thickness, the contact pressure between the current melt and the previous deposited layer is higher, leading to improved interlayer bonding and hence a more compact structure with reduced porosity. Additionally, printing more layers creates more opportunities for re-melting of the underlying area, thus promoting additional polymer diffusion and entanglement [57]. However, the increase of heating and cooling cycles when printing at small layer thickness can result in sample distortion, residual stress accumulation, and hence strength deterioration. Besides, parts printed with small layer thickness possess a higher number of interfaces which can potentially act as stress concentrations lowering the parts' mechanical performance [66, 67].

2.2.3 Raster width and raster angle

Raster width is the width of the deposition raster which is greatly influenced by the nozzle diameter. For FFF printing with large nozzle diameters, high melt flowrate and large raster width can be achieved to generate raster overlap, resulting in highly dense printed structures with high tensile strength [68]. However, it has been reported that printing at a smaller raster width could potentially enhance the mechanical properties of the FFF printed parts [69] as the surrounding area has more opportunity to be re-melted for stronger bonding

[57]. Raster angle is the direction of the deposition raster relative to the X-axis of the printer build platform. Generally, parts printed at 0˚ raster angle possess the highest tensile strength, while a 90° raster angle offers the lowest mechanical performance [67, 70]. This can be explained by the fact that all rasters in the parts printed at 0° orientation are pulled along their longitudinal axis, leading to tensile failure of the individual raster. However, when tensile loading is applied perpendicular to a raster's longitudinal axis, raster delamination occurs due to weak intra-raster bonding [67, 70]. Therefore, polymer parts are usually printed with bidirectional raster configurations such as [45˚/-45˚] or [0˚/90˚] to achieve more uniform mechanical properties independent of loading angle.

2.2.4 Air gap, infill density, and infill pattern

Air gap is defined as the gap between two successive rasters within a deposited layer, where its value can be zero, positive, or negative [71, 72]. For a zero air gap, the deposited material rasters are in close contact with each other. The rasters in the positive air gap, however, are deposited apart, resulting in a loosely packed structure, which is generally considered undesirable for high performance parts due to the potential property uncertainty associated with varying porosity contents. For the negative air gap, the adjacent rasters are deposited with an overlap, leading to a denser inner structure and, therefore, superior mechanical properties [72]. Notably, there is an optimum value for negative air gap to fabricate high-strength printed parts, because a negative air gap that is too large can reduce the parts' surface quality and dimensional accuracy due to excessive inter-raster overlap.

Regarding infill density, this parameter determines the amount of polymer material employed to fill space inside the contours and has direct impact on the mechanical properties as well as the mass of the printed parts. The value of this parameter is usually between 0 and 100%, in which 100% infill density corresponds to a completely solid part. A denser infill part usually possesses a higher strength due to more available polymer material for load-

bearing response [52, 58]. The infill pattern is the structure and shape of the infill offered by the slicer software. Different infill patterns such as grid, rectilinear, honeycomb, triangles, concentric, tri-hexagon, and gyroid can be used to form complex printed structures for specific applications [60, 73, 74]. Among these infill patterns, grid and lines are widely used patterns to fabricate printed parts with superior mechanical performance. This is due to the fact that highly dense printed structures can be achieved by employing these patterns, while their raster angle can be tailored to the dominant load application direction for improved load-bearing capability [60, 73].

2.2.5 Printing temperature

Printing temperature is the temperature at which the feedstock filament is heated during the FFF printing process. This printing parameter affects the viscosity of the material melt and the print quality. Usually, parts printed at high printing temperature possess higher tensile strength as the material melt maintains its temperature above the crystallization temperature and/or glass transition temperature for a longer time period for enhanced polymer diffusion [30, 64, 75]. However, excessive heating temperature can also lower the dimensional accuracy of the printed parts due to the lower melt viscosity [76] and is expected to unnecessarily increase energy consumption.

2.2.6 Build orientation

Build orientation describes the way through which the printed component can be oriented along the major axes of X, Y, and Z in the build envelope, referring to Fig. 2b. Tensile specimens of various build directions are generally tested to identify the anisotropy of the mechanical properties. For the 3D tensile specimen geometry printed in the XY (flat) and XZ (on-edge) orientations, the polymer rasters are mainly deposited in tensile load direction (X axis) [67, 73]. However, the XY specimen is built on a larger surface, while the XZ one is

built on a smaller edge on the XY plane. Regarding the ZX (upright) orientation, all the deposited layers are stacked in the Z direction which is also the tensile load direction. Most research studies have reported that tensile strength of the samples printed in XY and XZ orientations depends mainly on the strength of the feedstock materials, while the strength of those printed in ZX orientation (Z-strength) is strongly determined by the inter-raster bonding strength controlled by fusion bonds between the adjacent rasters [77]. Therefore, the Z-strength of the printed parts is always lower than the others since the inter-raster bonding strength is always weaker than the material strength [57, 75, 78-80]. It should be noted that polymer parts are usually designed according to their lowest properties to account for varying load directions and hence more attention needs to be paid to improve the Z-strength of FFF printed parts.

As most process parameters have a significant effect on the tensile strength of the FFF printed parts, many research studies have been conducted to optimize these parameters for printing parts with high mechanical performance. Reviews of this approach have been presented comprehensively in several papers [32-36, 67, 81, 82], and this approach is therefore not the focus of this review paper. Notably, the tensile strength achieved by this method is limited by the printers' capability and properties of the commercially available feedstock materials. To overcome these inherent limitations, process improvement approaches have been the recent focus of a large number of research groups to enhance the printed parts' strength further for high load-bearing applications. Our review paper groups these studies according to their main approaches involving either material developments, post-printing treatments, or process modification. The different approaches are reviewed and evaluated in terms of their underlying fundamental mechanism in the following sections.

3. Material modification for improved mechanical properties of FFF printed parts

Material modification is a popular method to improve the mechanical performance of FFF printed parts. For this approach, material components or fillers with desirable properties such as superior mechanical properties, fast diffusion rate, or low viscosity are introduced into the neat polymer feedstocks to enhance the performance of the resulting FFF printed parts. These new material systems for FFF process can be classified into three main groups: material blends, discontinuous filler-reinforced composites, and continuous fiber-reinforced composites.

3.1 Material Blends

3.1.1 Fabrication of blend filaments

Material blending is one of the most commonly used methods for modifying polymer materials. By combining polymers with different properties, the resulting material blend is designed to possess synergistic advantages compared to the individual materials, especially for mechanical properties [31]. Fig. 3 illustrates two main methods to fabricate FFF blend filaments: wet method (black arrow process) and dry method (red arrow process). In the wet method, different polymers in forms of granules, pellets, or powders are dissolved and mixed in solvents to form a homogeneous solution. The solvents are then evaporated, and the resulting product is dried and grinded to form blend granules. These granules are employed as the feedstock for the final melt-extruding process to produce FFF blend filaments [83, 84]. However, due to the use and disposal of large amounts of organic solvents, this method is environmentally unfriendly and considered more suitable for small-scale fabrication process.

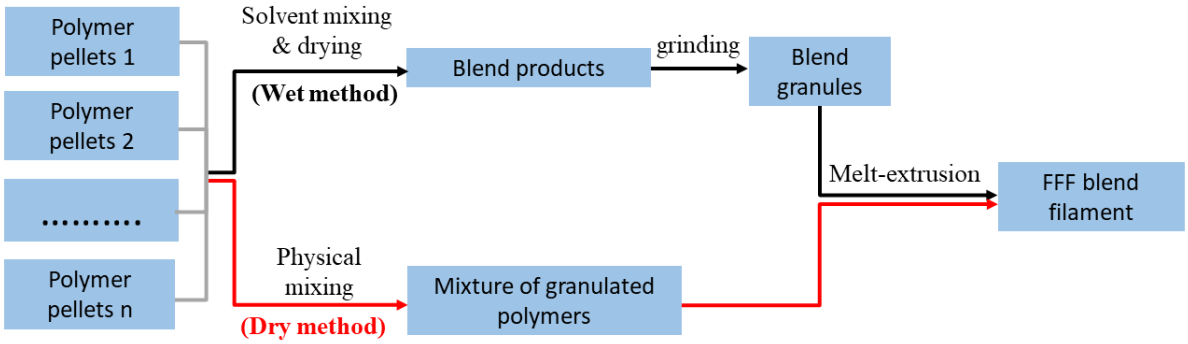

Fig. 3. Diagram illustration of fabrication process of FFF blend filament: wet method (black arrow process) and dry method (red arrow process).

The dry method, however, can address these issues by avoiding the use of organic solvents. In this method, the polymer components are physically mixed to form polymer mixtures before they are melt-extruded to form the final FFF blend filaments [85, 86]. The polymer mixtures can also be melt-blended or compounded and then extruded to produce blend filaments with a more uniform distribution of polymer components. Co-rotating twin screw extruder melt processing is widely used in the dry approach to fabricate the FFF blend filaments, especially for those with complex structures such as core-shell filaments [85, 87-92]. Since no solvents are used in this process, the dry method is eco-friendlier and more suitable for bulk production compared to the wet method.

3.1.2 Blending strategy for mechanical improvement of FFF printed parts

a) Blends with high-strength polymer components

Many studies of blends in FFF process have focused on improving elongation and fracture toughness of the printed parts. Usually, the additional polymer components are more ductile, but have lower mechanical performance than the neat polymers, resulting in a final blend with lower strength [86, 93]. However, several studies have also reported FFF-printed blend parts with improved tensile strength by combining the neat polymers with high-strength components. Rasselet *et al.* incorporated Joncryl®, a multifunctionalized epoxide, into a

PLA/ polyamide 11 (PA11) blend at 80/20 wt.% to slightly enhance the blend properties [94]. At 2 wt.% of Joncryl, the tensile strength and Young's modulus of the resulting printed blend parts obtained an enhancement of 22% and 21.4%, reaching 58.8 MPa and 3,376 MPa, respectively (Fig. 4a). This was explained by the fact that stress transfer efficiency between the PA11 dispersed phases and the PLA matrix was significantly improved as their stronger interfacial adhesion was formed through reactive compatibilization with the Joncryl, evidenced by the elongation of the PA11 dispersed phases observed in Fig. 4b.

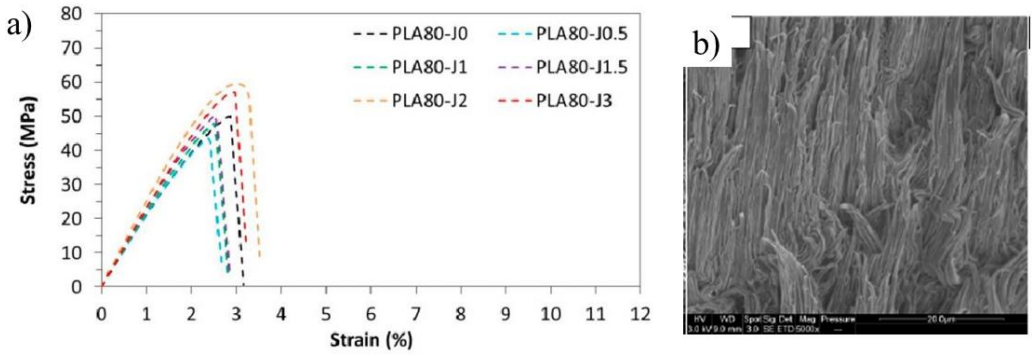

Fig. 4. (a) Stress-strain curves of FFF printed PLA/PA11 80/20 wt./wt. blends containing 0 to 3 wt.% of Joncryl. (b) Fracture surface of PLA/PA11 80/20 wt./wt. blends containing 2 wt.% of Joncryl. Reprinted with permission from Ref. [94].

b) Blends with reversibly crosslinked polymers

Diels–Alder (DA) chemistry is one of the novel material approaches to address the weak interlayer strength of the FFF printed parts [42]. Some Diels–Alder reactions are thermally reversible at high temperatures, allowing the polymers to be reversibly crosslinked as thermosets at low temperatures, but possess melt-processable properties as thermoplastics at high temperatures. Davidson *et al.* developed cross-linked polymers containing furan-maleimide Diels−Alder (fmDA) functional groups, which exhibited reversibility at typical FFF printing temperatures [83, 84]. Fig. 5a shows the synthesis process of the cross-linked fmDA-polymers, denoted as the mending agent (MA) [84]. The mole ratio of the monomers

for the MA synthesis (2M : 2F : 3F) was varied to control the cross-link density in the range of 0 to 100%.

In their first study, the fmDA polymers with 5% cross-link density were blended in ratios of 10 and 25 wt.% with PLA to produce blend filaments for FFF printing [84]. Interestingly, the resulting printed parts showed significant improvements in mechanical properties in XZ and ZX directions, although the strength in XY direction remained unchanged. Specifically, the samples printed by the 25% remendable PLA blends showed an improvement of 130% in ZX-strength and 27% in XZ-strength. Moreover, the toughness of the blends in all directions also increased significantly with improvements of up to 460%. In their later work, both strength and toughness in all directions of the parts printed by the 25% remendable PLA blends improved significantly with increasing cross-link density [83], as shown in Fig. 5b. At 100% cross-link density, the improvements for strength and toughness in ZX direction were the highest, reaching ~290% and ~1150%, respectively.

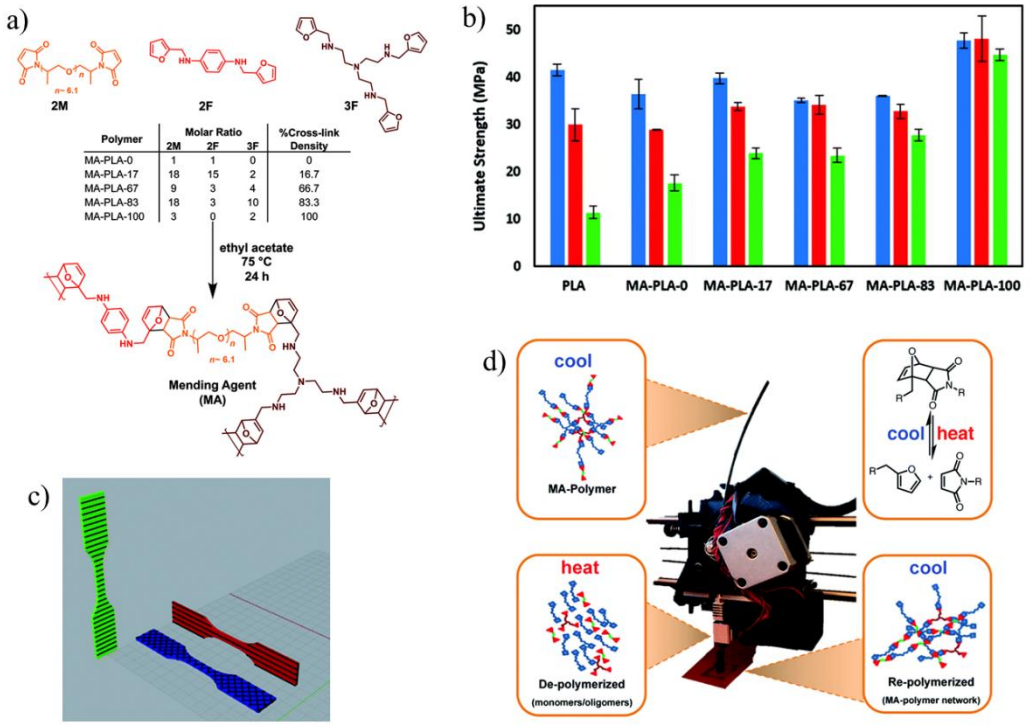

Fig. 5. (a) Synthesis of the Mending Agent (MA) polymers. (b) Ultimate strength of PLA and MA-PLA blends with varying cross-link density as dogbones for each print pattern. (c) Illustration of the three representative print orientations of dogbones; XY (blue), XZ (red), and ZX (green) along with their infill patterns. (d) Illustration of the thermoreversibility of MA-polymers during the FFF 3D printing process. Reprinted with permission from Ref. [83].

The impressive enhancement in both tensile strength and toughness of the MA-PLA blends is explained by two mechanisms presented in Fig. 5d [83, 84]. First, the retro-DA reaction at high temperatures (> 120 °C) allows the melted polymer to flow freely thanks to the broken cross-links between the MA polymer chains in the blend. Additionally, the breaking of the linear polymer chains reduces the molecular weight and lowers the melt viscosity, resulting in improved diffusion between the polymer melt and the deposited polymer layers during the FFF printing. Finally, the DA adduct formation during the cooling process (<60 °C) reproduces the MA polymer network in the blend, leading to the formation of new cross-links between the filament layers for improved interfacial strength. Notably, vitimers, a new class of polymer materials, also possess thermal reversibility behaviors at high temperatures and could be potential components for FFF blend filaments [95].

c) Blends with low molecular weight surface segregating additives

The low molecular weight surface segregating additive method addresses the poor interfacial adhesion between the deposited layers of FFF printed parts from a molecular level perspective [43, 96]. In a typical FFF deposition, the diffusion of large and bulky chains of the neat polymers between the filament interfaces is usually slow, while available thermal energy for the diffusion of the polymers between the filaments is limited, leading to poor interfacial adhesion. This polymer diffusion issue can be addressed by introducing low molecular weight surface segregating additives (LMW-SuSAs) into the FFF polymer

filaments. Since the LMW-SuSAs additives diffuse across the filament interface faster than the bulk polymers of the FFF filaments, the entanglement of the chains between the layers can be improved to achieve stronger interfacial bonding if their chains are sufficiently long.

Levenhagen *et al.* fabricated bimodal blend filaments consisted of high molecular weight PLA and low molecular weight (LMW) PLA additives (Mw ~26 – 44 k) for FFF printing [43]. The LMW PLA additives of 2-arm (linear), 3-arm, and 4-arm PLA stars (Mw of arm- ~11 k) were blended with the neat PLA at loadings of 3, 10, and 15 mol%. The viscosities of all blends were measured at the temperature used for FFF printing (190 °C) with a constant steady shear rate of 0.01 s^{-1}. The results showed that the mechanical properties of the printed parts improved after the introduction of 3 mol % of LMW PLA, but reduced with further increased LMW PLA loading (Fig. 6a). The improved mechanical performance of the printed parts in longitudinal direction at low additive concentrations was due to the reduced stress concentrations in the printed parts after the favourable migration of the LMW PLA to the interface of the deposited filaments. Regarding the strength in transverse orientation, the LMW additive at 3 mol % increased the number of entanglements across the interface and, therefore, enhanced the interlayer adhesion. However, at high loadings of LMW additive (10 and 15 mol %), the number of entanglements across the interface were saturated. Therefore, the interlayer adhesion was weakened at these loadings as the additive had lower strength and could not withstand high levels of mechanical stress [43].

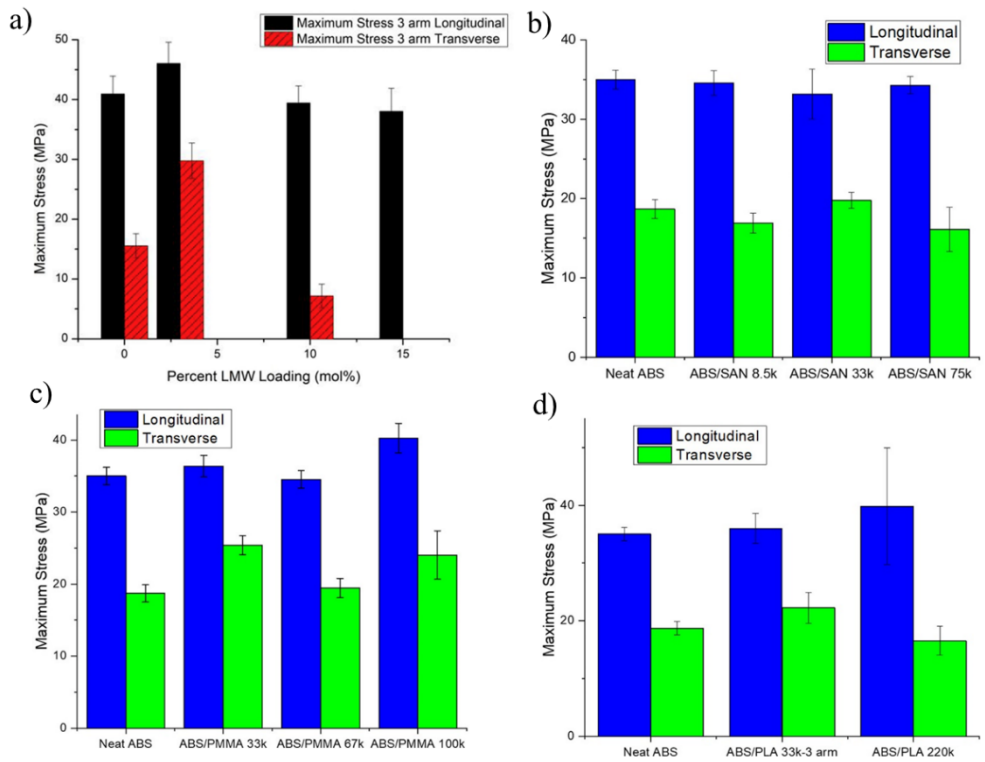

Fig. 6. (a) Tensile strength of PLA bimodal blend containing 3–arm PLA stars at different LMW loading. Reprinted with permission from Ref. [43]. Tensile strength of (b) ABS/PMMA, (c)ABS/SAN, and (d) ABS/PLA blends. Here, the addive loading is 3 mol %. Reprinted with permission from Ref. [96].

At 3 mol % loading, the mechanical performance in the transverse orientation of the printed parts increased significantly by 100% when the arm number of the LMW additive increased from 0 to 3, followed by a dramatic reduction of 43% at 4-arm LMW additive. It was found that all LMW additives reduced the viscosity of the PLA matrix, resulting in faster diffusion of polymers into the interface of the deposited filaments and increased entanglements for improved interfacial bonding. The 3-arm star polymers with unique architecture, however, had the lowest viscosity and therefore flowed more easily than the others. Besides, the foldability of their third arm allowed the formation of a pseudo-linear structure, leading to diffusion by reptation in a similar manner to 2-arm LMW additives. Importantly, their additional arm could generate more entanglements after the diffusion

process and achieve an improved interlayer bonding compared to pure 2-arm polymers, resulting in a significant decrease in the anisotropy of the printed part [43].

In a later research work, Levenhagen *et al.* extended this methodology to ABS systems to study the mechanism of interfacial strengthening [96]. In their study, neat ABS polymers were blended with LMW-SuSAs additives of PMMA (33k, 67k, and 100k), SAN (8.5k, 33k, and 75k), and PLA (33k-3 arm and 220k) at a loading of 3 mol %, and the mechanical performance of their printed FFF parts was studied. Notably, these three materials were selected based on a continuum of their chemical similarity and miscibility to the matrix polymers: SAN is the most miscible and chemically similar to the ABS matrix. Both PMMA and PLA are chemically different from the ABS phase. However, PMMA is miscible, while PLA is immiscible to the ABS constituents. Figs. 6b-d present the mechanical strength of all resulting blends. As can be seen, the addition of the 33k LMW SAN only increased the transverse strength of the blend slightly, while impressive improvements of 40% and 25% were achieved by the blends with the 33k PMMA and 33k- 3 arm PLA, respectively. These results stemmed from the surface segregation of the LMW additives to the interface of the deposited filaments and the increase in the number of entanglements between the adjacent filaments.

3.1.3 Mechanical improvements of FFF printed parts by material blending

In this review paper, improvement efficiency index (IEI) is introduced to normalize and compare the efficiency of different property improvement methods. This index is defined as the ratio of the mechanical properties of the printed parts achieved after applying the process improvement method and their initial as-printed properties (Eq.1).

$$Improvement\ efficiency\ index = \frac{Achieved\ mechanical\ property}{Initial\ mechanical\ property} \qquad (1)$$

Fig. 7 shows the calculated IEI values versus achieved strength and Young's modulus of FFF printed blend parts reported in literature. Each data point on the graphs is located by its tensile strength / Young's modulus of the polymer parts achieved after applying respective property improvement methods (X-axis) and its calculated IEI value related to the initial as-printed mechanical property of the coupons produced via benchmark FFF processes (Y-axis). In addition, the data points of unfilled circle and filled diamond symbols with the same colors represent properties in the longitudinal (XY) and transverse (ZX) directions of parts reported from the same research work, if both are available. Therefore, their differences in X values (achieved mechanical properties) also indicate the anisotropic degree of the printed parts.

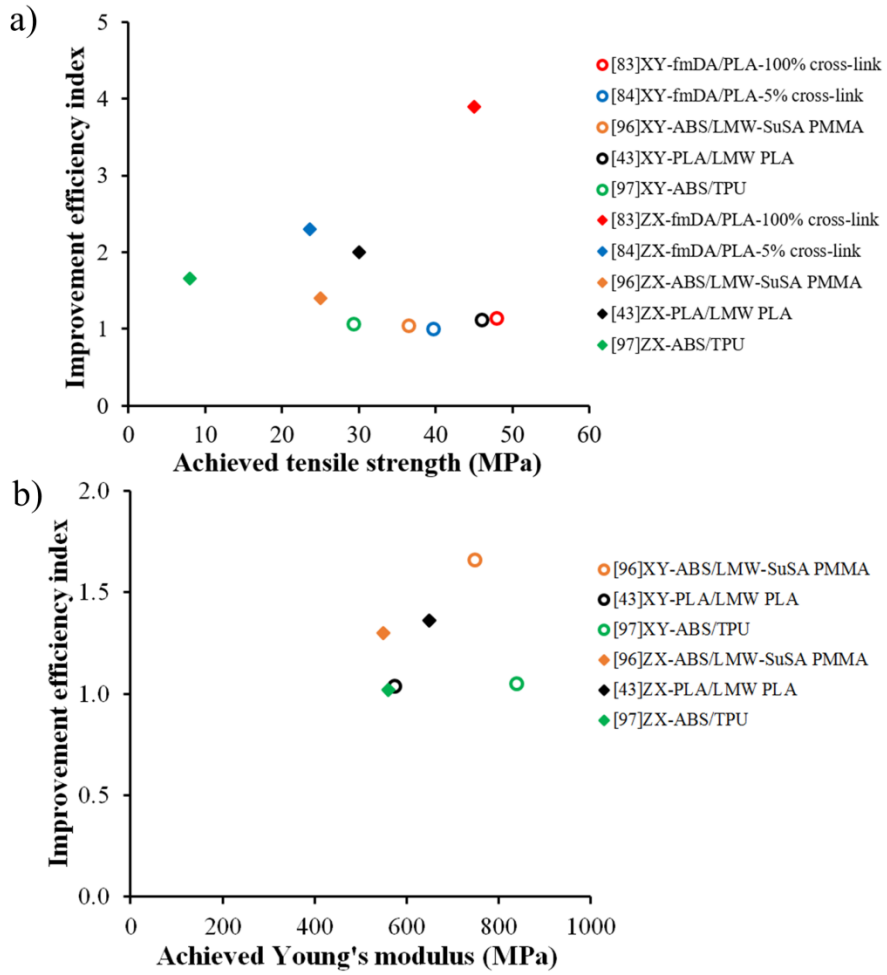

Fig. 7. Plots of (a) IEI value of tensile strength versus achieved strength and (b) IEI value of Young's modulus versus achieved Young's modulus via material blending.

As can be seen, most of the blend strategies focus mainly on improving the Z-strength of the FFF printed parts [43, 83, 84, 96, 97]. Specifically, the 5 highest IEI values achieved by the blend approach are for the Z-strength, ranging from 1.4 to 3.9 times. Among the reported methods, the approach of reversibly cross-linked polymers possesses the best efficiency with the highest IEI values for the tensile strength of fmDA/PLA in transverse (3.9 times) and longitudinal (1.14 times) orientations, reaching 45 and 48 MPa, respectively (nearly isotropic) [83]. The blends of ABS/TPUs exhibit the lowest IEI values for both strength and Young's modulus (below 1.6 times) [97]. Overall, IEI values of less than 2 times in Young's modulus for both transverse and longitudinal directions are produced by this approach, as shown in Fig. 7b.

3.2 Discontinuous filler-reinforced composite

Similar to the polymer blending approach, discontinuous fillers such as short fibers, sheets, or particles in micro- or nano-sizes can be integrated into neat polymer filaments to enhance the mechanical performance of the FFF printed parts. Although several discontinuous filler composite filaments, such as graphene/PLA, wood/PLA, iron/PLA, carbon fiber (CF)/ABS, CF/PLA, glass fiber/ABS, and CF/nylon are commercially available, they are generally more costly and their compositions are limited. As a consequence, the researchers for most studies of FFF printed polymer composites fabricate their own composite feedstock filaments for specific applications due to the design freedom of the filament compositions and materials.

3.2.1. Fabrication methods of discontinuous filler-reinforced composite filaments

Fig. 8 presents three main methods to fabricate discontinuous filler-reinforced composite filaments for FFF process: solvent-based method (black arrow process), melt-based method (red or green arrow process) and dilution-based method (yellow arrow

process). For the solvent-based method, a dispersion of polymer and discontinuous fillers is formed by dissolving and mixing them in solvents. The dispersion is then cast to remove the solvents by evaporation and to form composite products. These are then ground into composite granules prior to extruding to produce final composite filaments for FFF printing [98, 99]. Similar to the wet method of the blend fabrication, the solvent-based method is generally not classed as environmentally friendly and mainly used in laboratories for small-scale processing. In addition, the polymer can degrade after being dissolved in the solvent mixture, thereby lowering the performance of the final printed parts.

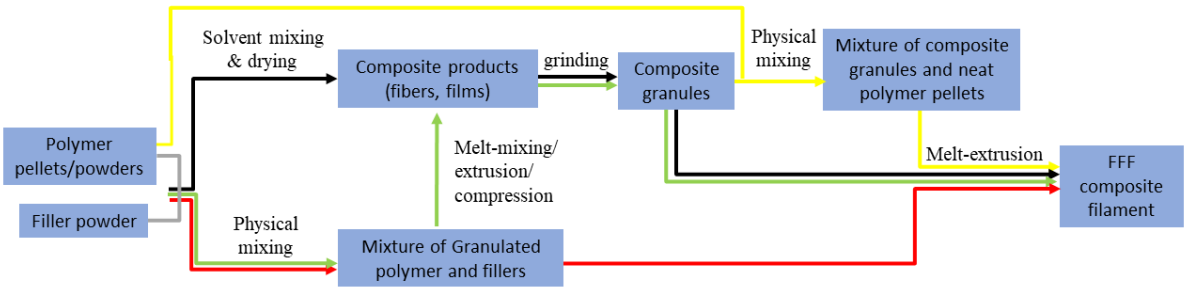

Fig. 8. Diagram illustration of fabrication process of FFF discontinuous filler-reinforced composite filaments: Solvent-based method (black arrow process), melt-based method (red or green arrow process), and dilution-based method (yellow arrow process).

The melt-based method involves physically mixing or blending polymer pellets and discontinuous fillers at room temperature to form a dry mixture. The mixture can be directly loaded to an extruder for final filament extrusion. However, it also can be melt-mixed and processed into composite products such as composite films or filaments to enhance the quality and uniformity of the mixture. Alternatively, this step can be conducted by employing a twin screw extrusion process in which filler loading can be controlled by tailoring the respective flow rate of both polymers and fillers. These composite products are then ground to produce composite granules before their final melt extrusion to produce FFF composite filaments [100, 101]. Notably, multiple thermal and mechanical exposures of the polymers

during the filament fabrication can result in thermal and mechanical degradations [102]. These are common issues in polymer extrusion process and can be addressed by using thermal stabilizers and processing aids [103].

Similar to the dry method of the blend fabrication, the melt-based method is considered eco-friendly and suitable for bulk production. However, this method is more likely to introduce damage to the fillers due to the interactions between the fillers and the instrument surfaces during the mixing process. Therefore, the fabrication process has to be designed and optimized properly to minimize filler attrition. Regarding the dilution-based method, the granules fabricated from the composite fibers/films with high concentration of discontinuous fillers are physically mixed with the neat polymer pellets to achieve a composite mixture with lower filler volume fraction before melt-extruding to form FFF composite filaments [104, 105]. This method can address the dispersion issues of the discontinuous fillers as the composite products with high concentration of fillers can be commercially available or can be fabricated in advance by either the solvent-based or the melt-based methods.

3.2.2. Effects of filler loading on void formation and mechanical properties of FFF printed discontinuous filler-reinforced composite

Similar to conventional composite characteristics, the mechanical strength of the FFF printed composite is strongly determined by the interfacial bonding between the reinforcing fillers and the polymer matrix as well as the homogeneity of the filler distribution [106]. For short fibrous fillers, a higher orientation in both fillers and polymer molecules can be achieved in the FFF printed parts due to the flow-induced effects of the extrusion process compared to other conventional fabrication processes [77, 107, 108]. Besides, void formation and filler loading also play crucial roles in their mechanical performance.

a) Effects of filler loading on void formation in the FFF printed discontinuous filler-reinforced composite

The introduction of discontinuous fillers into filament feedstock can decrease the die-swell effects significantly, leading to smaller rasters and, hence, smaller inter-raster gaps [109]. Moreover, high conductive fillers such as CF, carbon nanotubes (CNTs), graphene, and Al enhance the thermal conductivity of the composite rasters significantly [99]. This not only reduces the warpage issue of the FFF print [77], but also improves the polymer diffusion efficiency between the deposited composite rasters, resulting in a higher packing and smaller gaps of the printed parts. Tekinalp *et al.* reported that lesser pores and gaps were observed in the cross-sections of CF/ABS printed parts after short carbon fibers were integrated into ABS filaments [109], as can be seen in Figs. 9 a-b. However, higher CF loading produced more pores and gaps (Figs. 9b-d), with pore enlargement around the fibers in the FFF printed samples (Fig. 9e). This is explained by the fact that the increasing number of filler generates more intra-raster voids at the edges of or around the fillers since the fiber filler and the polymer matrix flow partially independently during the printing process [109].

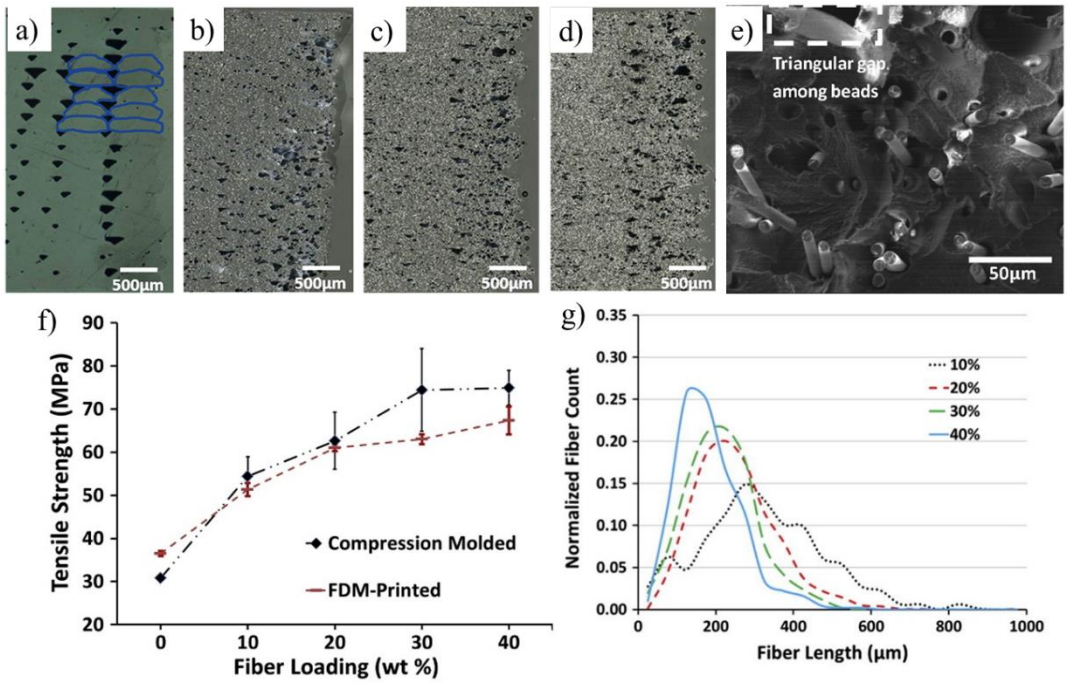

Fig. 9. Cross-sections of CF/ABS printed parts with (a) 0 wt.% CF, (b) 10 wt.% CF, (c) 20 wt.% CF, (d) 30 wt.% CF. (e) Fracture surface of 10 wt.% CF-loaded ABS printed parts. (f)Tensile strength of parts fabricated by compression molding and FFF at different fiber loading. (g) Fiber length distribution in printed CF/ABS parts at different fiber loading. Reprinted with permission from Ref. [109].

These voids reduce the fiber–matrix interfacial contact area, weaken the interfacial bonding, and lower the mechanical properties of the printed composite parts. The intra-raster porosity can be reduced by enhancing the compatibility and attachment of the fillers and the matrix via applying surface treatment to the fillers or employing suitable sizings before the FFF printing. Generally, the void volume fraction in the FFF printed parts with the discontinuous filler-reinforced composite results from the competing changes between the large voids among the rasters (inter-raster porosity) and the smaller voids inside the rasters (intra-raster porosity) with increasing filler concentration [109].

b) Effects of filler loading on the mechanical properties of the FFF printed discontinuous filler-reinforced composite

Similar to conventional composite materials, integration of reinforcing fillers into FFF filaments enhances the mechanical performance of the printed parts significantly. However, there is an optimum filler loading for the FFF printed composite parts to achieve the highest tensile strength and Young's modulus due to the competing effects between reinforcing efficiency of the fillers and void formation. For example, Tekinalp *et al.* reported an increase of up to 115% in the tensile strength of CF/ABS printed parts, reaching 70 MPa when CF loading increased from 0 to 40 wt.% [109], as shown in Fig. 9f. However, the optimum concentration of CNT fillers in CNT/ABS printed parts reported by Thaler *et al.* was only 5% [104]. This optimum value varies significantly in different reported studies, mostly due to the

variation in the filler types, filler distribution condition, and interfacial bonding strength between the fillers and the polymer matrix [77].

At loading contents below this optimum value, the fillers can be dispersed homogeneously into the polymeric matrix and the void formation caused by filler introduction is still low. Consequently, high filler-matrix bonding strength can be achieved, leading to superior mechanical properties of the printed composite. Some research studies also reported the improvement in mechanical properties in transverse orientation of the FFF printed parts owing to the reinforcing effects of fillers at the inter-filament interfaces [110], along with enhanced polymer molecular diffusion and entanglements across the interface due to improved thermal conductivity of the printed composite parts at low filler loading [99]. However, too high loading of the discontinuous fillers produces more pores within the printed parts, owing to inhomogeneous dispersion of the fillers into the polymer matrix or the significant increase of intra-raster porosity, hence reducing the load transfer efficiency between the fillers and the polymer matrix [77, 104, 109].

Besides, introduction of more fillers into the polymer matrix can increase the viscosity of the melt material, leading to reduced inter-filament polymer diffusion. Similarly, the fillers segregated at the interface with high loading may hinder inter-filament diffusion and act as stress points that generally weaken the interface and reduce polymer chain entanglements [77]. Additionally, due to the increased interactions between the fillers, instrument surfaces, and matrix polymers at high filler loading, the filler size reduces significantly as the fillers are damaged more severely during compounding and extruding process. For example, Tekinalp *et al.* reported a reducing trend of average carbon fiber filler length when the fiber loading increased (Fig. 9g), although a much longer fiber length (~3.2 mm) was initially used [109]. The damaged and smaller reinforcing fillers provide lower reinforcement effects to the composite printed parts, leading to lower mechanical

performance. Therefore, modification/optimization of both mixing and printing processes to minimize the filler damage and intra-pore formation plays a crucial role in improving the mechanical properties of the printed composite parts.

Additionally, the filler loading needs to be optimized for processability, because high filler concentrations reduce the flowability of the composite melt as a result of their high viscosity, while increasing nozzle clogging issues [111, 112]. Moreover, it is difficult to produce continuous composite filaments with high filler loading owing to the loss of toughness. Therefore, it is necessary to further understand the rheological properties of the printing composite materials and increase the filler content to achieve optimal mechanical strength of the FFF printed parts [113-115]. Also, the effects of different fillers on mechanical properties of polymer parts fabricated by FFF process vary with different polymer types and a review on this issue can be found in several papers [30, 77, 106]. Similar to conventional composites, the composite parts printed via discontinuous filler-reinforced composite approach also experience a decrease in elongation and toughness with increasing filler loading [77, 104, 109].

3.2.3 Mechanical improvements of FFF printed parts by discontinuous filler-reinforced composite approach

Fig. 10 presents IEI values of tensile strength and Young's modulus for the approach of discontinuous filler-reinforced composite. As can be seen, most research work mainly reported the improved mechanical properties in longitudinal direction [98-101, 104, 105, 109, 116-123]. Among the fillers used in this approach, short carbon fibers provide the best reinforcement effects, with IEI values of up to 2.15 times for tensile strength and 8 times for Young's modulus. In addition, its achieved strength and Young's modulus are among the highest, reaching 70 MPa and 9.28 GPa, respectively. This is attributed to the alignment of the fibrous fillers along the longitudinal direction thanks to the flow-induced effects [77].

Only PMMA/Si composite shows a comparable IEI value of 2.37 times for tensile strength, but its absolute achieved strength is only 41.8 MPa.

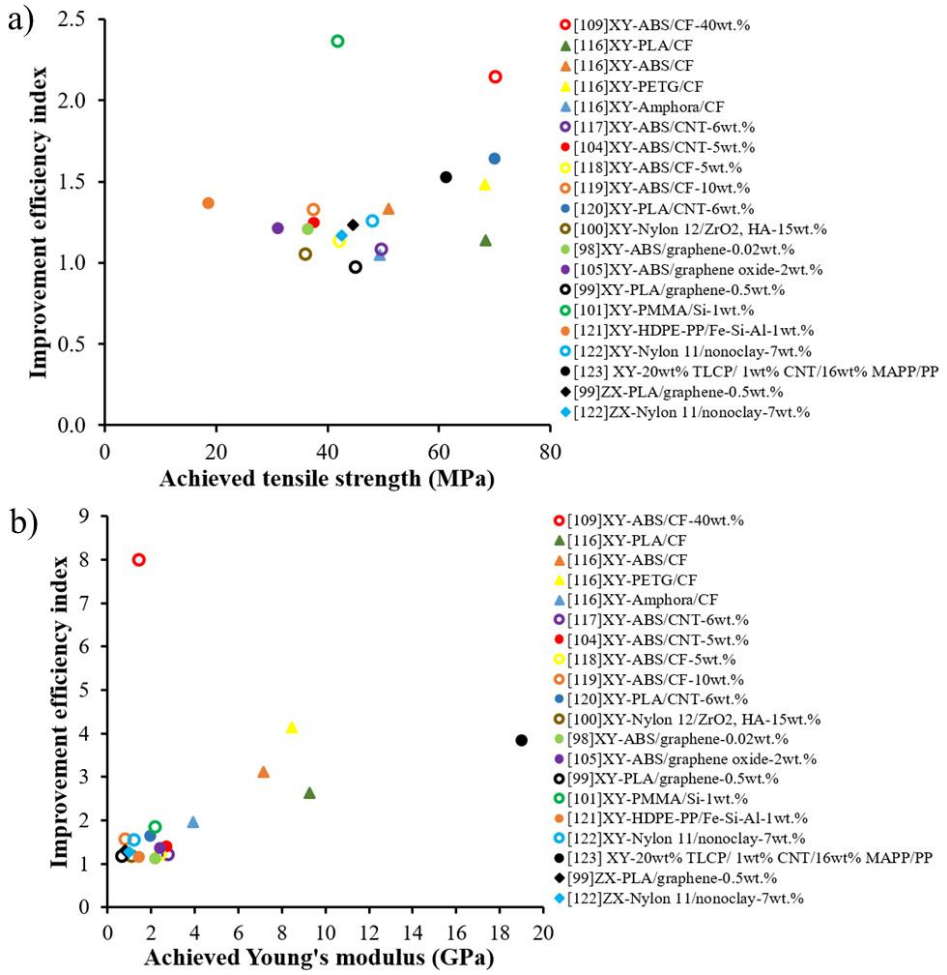

Fig. 10. Plots of (a) IEI value of tensile strength versus achieved tensile strength and (b) IEI value of Young's modulus versus achieved Young's modulus via the discontinuous filler-reinforced composite method.

3.3 Continuous fiber-reinforced composite

In this approach, continuous reinforcing fibers and polymer matrix are directly fed into a FFF setup to fabricate high-strength composite printed parts. Similar to the discontinuous filler-reinforced composite approach, the mechanical strength of the FFF printed composites in this method is strongly determined by the strength and interfacial bonding of both reinforcing fibers and polymer matrix [31, 41, 107, 124]. To achieve an

efficient interfacial bonding, two types of physical setups are generally employed: one-nozzle approach for simultaneous feeding [76, 125-130] and two-nozzle setup for separated deposition of reinforcing fibers and polymer matrix [131-140].

3.3.1 Approaches for FFF printing of continuous fiber-reinforced composite

a) One-nozzle approach

In this method, the FFF process is modified so that continuous reinforcing fibers (CRFs) can be impregnated in the thermoplastic melt pool inside the printer nozzle before the resulting composite materials are extruded simultaneously [76, 141]. Fig. 11a illustrates a schematic of a FFF printer with a one-nozzle setup for printing continuous fiber-reinforced composites [76]. As can be seen, a polymer filament and reinforcing fibers are separately fed into a printer head. The polymer filament is melted by the heater inside the printer head, and the movements of the polymer melt generate shear stress at the surface of the reinforcing fibers when they contact each other inside the head. This helps to draw the reinforcing fibers into the printer head and, therefore, the fibers can be supplied to the printer head automatically without additional devices [126]. Then, the resin-reinforced fibers are extruded from the nozzle and deposited onto a printing bed to fabricate solid parts, similar to the conventional FFF process. During the printing process, the already extruded melt stuck on the print bed/printed parts also provides persistent traction force to pull the reinforcing fibers out of the nozzle [127].

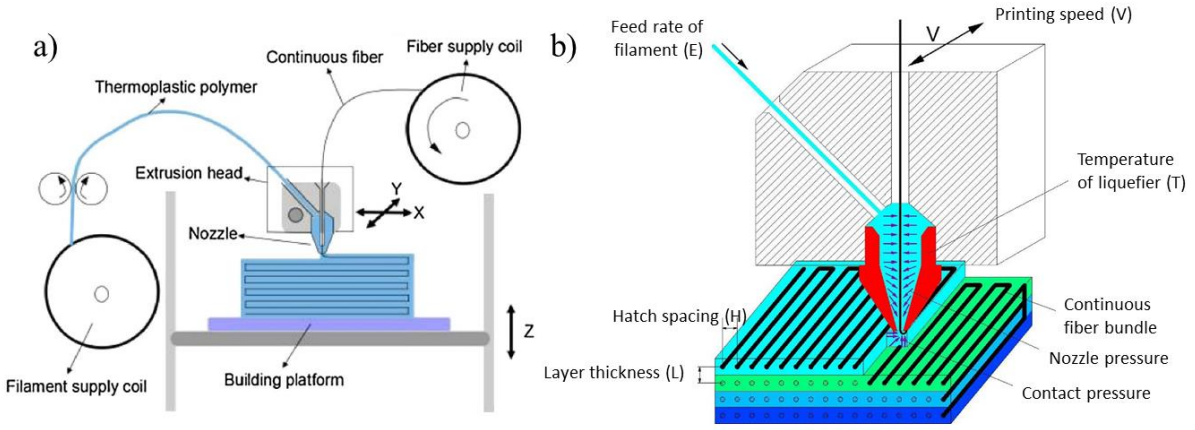

Fig. 11. Schematics of FFF printing process of continuous fiber-reinforced composite via one-nozzle approach (a) and its process parameters (b). Reprinted with permission from Ref. [76].

The 3D printers for fabricating continuous fiber-reinforced composite via the one-nozzle setup are developed by modifying the printer head of the commercially available FFF printers. Therefore, conventional printing parameters such as layer thickness, printing temperature, feed rate of filaments, hatch spacing, and transverse movements also play crucial roles in the performance and quality of the printed composite parts. Tian *et al.* reported a comprehensive study of different printing parameters on the mechanical properties of printed continuous CF/PLA samples [76], as shown in Fig. 11b. Their study showed that printing temperature has considerable effects on the impregnation of the reinforcing fibers and the polymer matrix as well as the interfacial bonding strength between the deposited layers. When the printing temperature is too low, it is difficult to extrude the composite material owing to the poor flowability. Additionally, interfacial bonding between the deposited layers is insufficient at low printing temperature, leading to delamination failure and lower mechanical strength. However, at too high printing temperature, the printed parts lose surface finish and dimensional accuracy due to the overflow of the melt polymer. Only the optimum printing temperature provides the required flowability to the heated composite material for high impregnation between the polymer melt and the reinforcing fibers, leading

to drastic enhancements in the mechanical properties of the FFF printed composite parts. The optimum printing temperature varies with different feedstocks and is usually determined by process parameter optimization.

In the one-nozzle approach, layer thickness plays a crucial role in the accuracy, reinforcement efficiency (strengthening efficiency of the reinforcing fibers), and mechanical properties of the FFF printed composite parts. Since the amount of the reinforcing fibers in the extruded composite materials is unchanged, the layer thickness is mainly controlled by adjusting the amount of the polymer melt, thus determining the fiber volume fraction of the printed composite parts. Consequently, the composite parts with high volume fraction of the reinforcing fibers can be printed by reducing the layer thickness. Moreover, the decreased gap between the printer nozzle and the previous deposited layer improves their contact pressure when printing at a smaller layer thickness [142, 143], leading to stronger interfacial bonding between the deposited layers and, hence, improved mechanical properties [76].

Hatch spacing or air gap is also important parameter that determines the overlapping degree between the extruded melt and the already deposited layers, as shown in Fig. 11b. Similar to the layer thickness, the hatch spacing also affects the contact pressure between the nozzle and the deposited layer. In fact, large contact pressure can be achieved by reducing the hatch spacing to enhance the overlapping degree between adjacent rasters, resulting in improved mechanical strength of the printed composites [76]. However, too low hatch spacing produces excessive overlaps and disrupts the printing process. The feed rate of the filament is the unit volume of material fed into the printing nozzle. It determines the extrusion speed and the inner pressure of melt composite material in the printhead. When printing at a high feed rate, composite materials are extruded at larger volume. This increases the overlapping contact pressure between the deposited layers and the inner pressure in the liquefier, leading to superior mechanical performance. However, excessive increases in the

feed rate shorten the impregnation period for the reinforcing fibers and the polymer matrix in the printer head and thus lowers their interfacial bonding, which in turn causes layer delamination and poor mechanical performance.

The interfacial bonding issue can be addressed by modifying the surface of the reinforcing fibers before the printing process. Heidari-Rarani *et al.* modified the surface of CF bundles by adding PVA as sizing [127], as presented in Fig. 12a. In their study, CF roving was impregnated in a solution of PVA and water for 1 h at 60 ^{o}C. The impregnated roving was then passed through a die with a 1-mm hole to remove the excessive PVA and ensure circular cross-section before being dried at the room temperature. In another approach, Li *et al.* modified commercial CF bundles with PLA for FFF printing of CF/PLA composite by using the process shown in Fig. 12b [128]. In their study, PLA particles (8 wt.%) were partially dissolved in methylene dichloride solution after 30 min magnetic stirring. Then, the filtrate of the PLA resin in methylene dichloride solution was sheared and emulsified by using a high-speed dispersing and emulsification machine. A solution of emulsifying, antifoaming, and surface active agents were prepared at 1 wt.%. The solution was then slowly added to process the aqueous PLA sizing agent and modify the surface of the reinforcing CFs.

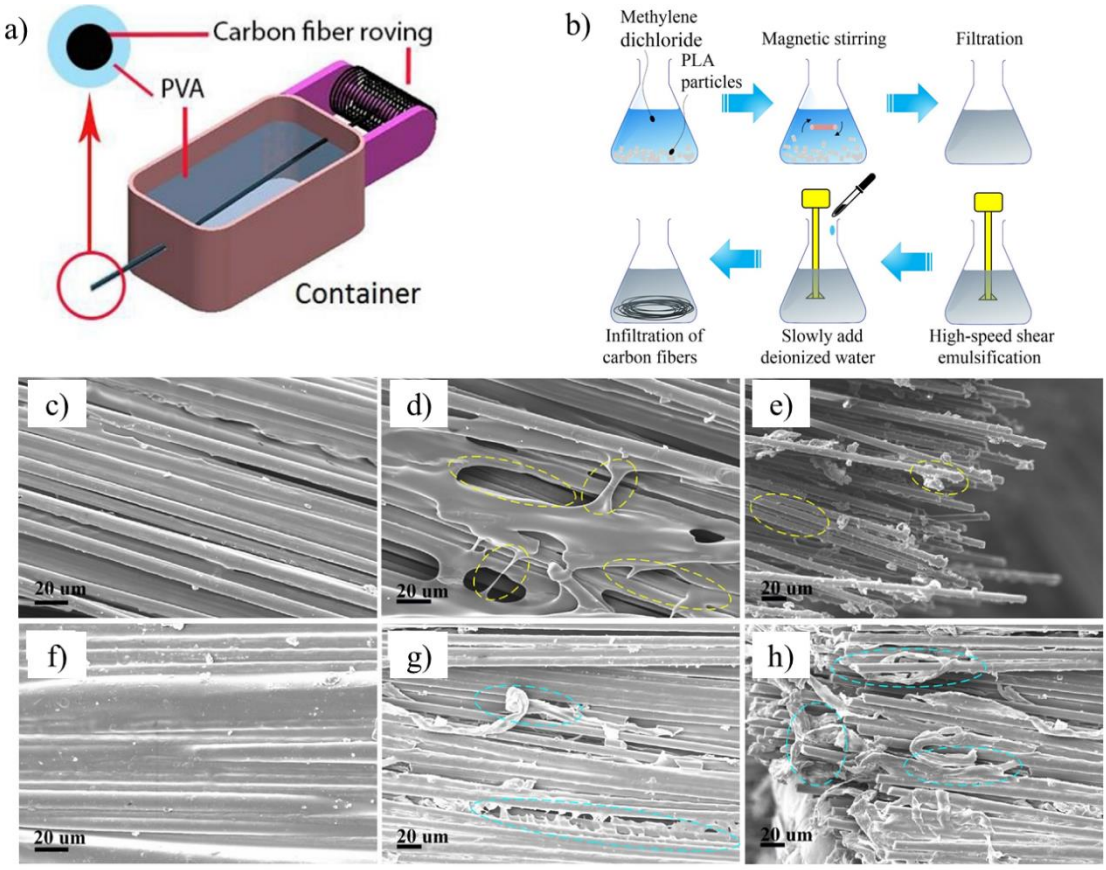

Fig. 12. (a) Surface preparation of CF roving with PVA. Reprinted with permission from Ref. [127]. (b) Surface preprocessing modification of CFs with PLA. SEM micrographs of printed composites: (c) Fiber-matrix interface of CF/PLA specimen. (d) CF/PLA specimen after tensile test. (e) Fiber pull-out of specimen after tensile test. Here, the yellow circles mark the regions of voids and small bridges with little PLA resin covering the cracked CFs. (f) Fiber-matrix interface of modified CF/ PLA specimen, (g) Modified CF/PLA specimen after tensile test. (h) Fiber pull-out of modified CF/PLA specimen after tensile test. Here, the cyan circles mark the regions of lower void content and a large amount of PLA resin covering the cracked CFs. Reprinted with permission from Ref. [128].

Consequently, the modified CF/ PLA printed samples exhibited a 14% improvement in tensile strength compared to the untreated CF/PLA printed counterparts. This was attributed to the improved interfacial bonding between the PLA matrix and the reinforcing CFs after the treatment. Figs. 12 c-h present SEM images of the CF/PLA samples with and

without surface treatment before and after tensile test. Compared to the unmodified printed parts, the surface modified samples possessed a nearly void-free microstructure with a more homogeneous distribution of PLA between CFs, indicating improved wetting and resulting stronger interfacial bond. Moreover, there were many PLA polymer clad among the cracked fibers without observed prominent separation of the modified fibers and the matrix. The results suggested that modifying the surface of CFs before the printing process is a promising approach to enhance the interfacial strength between the polymer matrix and the reinforcing CFs in the FFF printed composite [128].

b) Two-nozzle approach

In this approach, 3D printers with 2 nozzles are used: one nozzle is for the deposition of continuous reinforcing fibers pre-impregnated with matrix polymer and the other nozzle is for the extrusion of matrix material [131, 144-146]. The printers can also fabricate parts made of matrix materials if only the matrix nozzle is used for the printing process. Although a few commercial FFF printers with the two-nozzle setup can fabricate continuous fiber-reinforced composite, most studies reported in literature used Markforged 3D printers to print composite specimens. The reported system can print two kinds of materials independently as it has two extruders and two injectors [131], as presented in Fig. 13a. One of the injectors was used to print Nylon or short CF/Nylon composite, also known as Onyx™, and the other one was used to print a towpreg filament consisting of a bundle of long reinforcing fibers such as carbon, glass, and arimidic (Kevlar™) fibers pre-impregnated with thermoplastic resin. The printer used Eiger software for slicing STL and OBJ models to control the orientation of the reinforcing fibers as well as the stacking sequence of the polymer matrix and the reinforcing fiber layers [132].

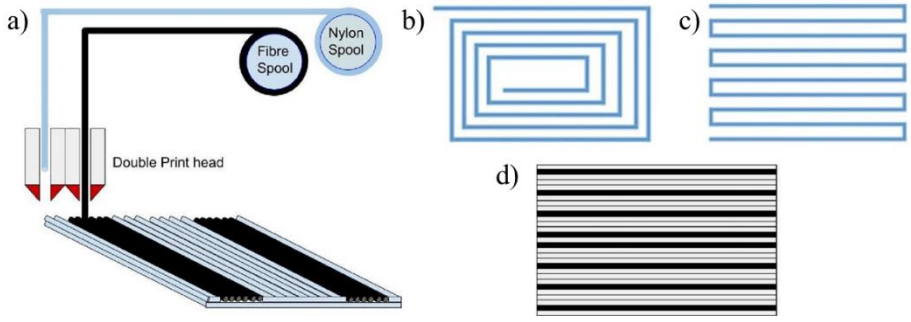

Fig. 13. Schematic of (a) FFF printing process of continuous fiber-reinforced composite via two nozzle approach, (b) concentric fiber pattern, (c) isotropic pattern, and (d) stacking sequence of fiber-reinforced (black) and nylon only (white) layers. Reprinted with permission from Ref. [131].

As shown in Figs. 13b and c, the reinforcing fibers can be deposited into 2 pattern types: concentric and isotropic. In the concentric pattern, the reinforcing fibers are deposited in a form of annular rings, and the ring number can be controlled via the software settings. Regarding the isotropic pattern, the reinforcing fibers are extruded in a unidirectional pattern to create continuous reinforcing lines in the entire layer at desired angles. The matrix is usually printed by the first nozzle at a temperature of approximately 270 °C onto a non-heated printing bed, and the printing process was similar to a conventional FFF [131]. The towpreg filament, however, was heated at a temperature higher than the melting temperature of the matrix material to melt it interstitially within the filament. The towpreg filament was fed through the second nozzle to deposit the material layer by layer into the desired shape, while a cutter was used to cut the filament after the printing layer was completed. Notably, Markforged printers are closed systems and most reported studies have employed the printing parameters optimized for processing only Nylon based materials. The main focus of the research on FFF printing using the two-nozzle setup is the build strategy of the printed composite, comprised of 3 main variables: (1) layer number of the matrix and the reinforcing fiber, (2) stacking sequence of the fiber layers and the matrix layers (Fig. 13d), and (3)

pattern configurations of the fiber layers including number of rings and starting point of fiber deposition for the concentric pattern and raster angle for the isotropic pattern.

Naranjo-Lozada *et al.* studied the effects of different printing architectures and the starting point of the fiber deposition in the concentric pattern on the tensile strength of CF/Nylon composite printed by Markforged printer [134]. The printed geometry is a Type I tensile bar following ASTM D638 with a total number of printing layers of 26, as presented in Figs. 14a-d. The number of CF layers (L) and ring number of each CF layer (R) were varied from 1 to 5 and from 2 to 18, respectively, creating different "printing architectures" with volume fractions of reinforcing fibers in the range of 0% to 54%. Additionally, 1R-12L samples were printed with different starting points of fiber deposition (outside, in middle, and uniformly distributed over the tensile area of the specimens) to study their effects on the mechanical performance of the printed parts. Fig. 14e shows the tensile strength of the CF/Nylon composite printed at different volume fraction and configurations. As can be seen, the tensile strength of the printed samples increased significantly with increasing volume fraction of the reinforcing fibers; while at the same volume fraction, the samples with higher ring number, but less fiber layers, possessed improved mechanical performance. Due to their highest volume fraction (54%), the 5R-18L samples exhibited the best mechanical strength (304.28 MPa) and Young's modulus (23.7 GPa).

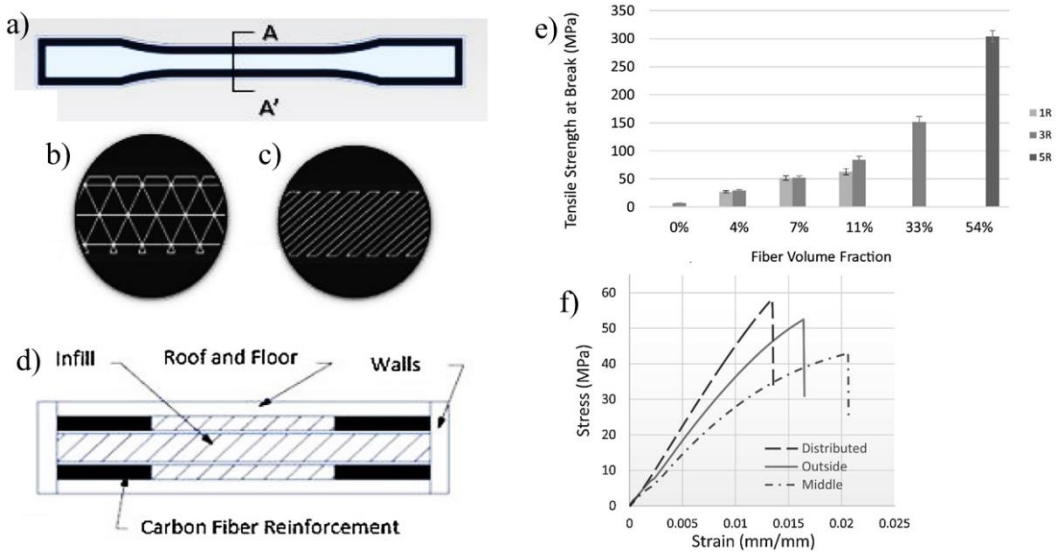

Fig. 14. Continuous Carbon Fiber-Reinforced specimen: (a) Top view, (b) Triangular Infill Pattern, (c) Rectangular Infill Pattern, and (d) Cross Section A-A'. (e) Effects of Fiber Volume Fraction and Printing architecture (1R, 3R and 5R) on tensile strength of CF/Nylon printed parts via two-nozzle approach. (f) Stress-strain curves of CF/Nylon composite at different start points. Reprinted with permission from Ref. [134]

Moreover, the starting point of the fiber deposition was found to have significant effects on the mechanical properties of the printed composite (Fig. 14f). The 1R-12L samples with reinforcing fiber ends located at the middle of the tensile area had the lowest strength with failure occurring at the starting point of the deposited fibers. In fact, the tensile strength and Young's modulus of the "middle" samples showed a decrease of 16.5 and 16.9%, respectively, compared to the "outside" samples. This low mechanical performance was attributed to lesser reinforcing fiber bundles to withstand the load at the starting point. However, the printed samples with distributed starting points over the tensile area exhibited the highest mechanical performance with an increase of 11.3 and 8.4% in tensile strength and Young's modulus, respectively, compared to the "outside" samples. It was found that the distribution of the starting points could release some compression stresses in the inflection area. This prevented the crack initiation as in the failure case of the "outside" samples, while

the small defects generated by the stacked distribution were not critical for failure occurring as in the “middle” samples’ failure [134].

In another study, Peng *et al.* investigated the effects of the stacking sequence on the mechanical behaviour of printed laminated composites made of short CF/Nylon composite as matrix and continuous CF towpreg as reinforcement [133]. For a total layer number of 10 layers, four continuous CF-reinforced (CCFR) layers with six short CF-reinforced (SCFR) layers (samples 4–1 and 4–2) and six CCFR layers with four SCFR layers (6-1 and 6-2) were printed in two different stacking sequences, as shown in Table 2. Notably, SCFR and CCFR layers were the white and gray layers, respectively. The results suggested that the printed samples with the separated CCFR layers exhibited superior mechanical performance compared to those with the agglomerated CCFR layers. Figs. 15 a-c show three different interfaces in the printed samples: interface between SCFR layers (S-S), interface between CCFR layers (C–C), and interface between SCFR and CCFR layers (C-S). As can be seen, the SCFR layers were tightly attached together without visible defects at the interface S-S, while voids were clearly observed at the other interfaces.

Table 2. Tensile strength, elastic modulus, and elongation at break for the printed laminated composites with different number and structure of CCFRLs (gray color) and SCFRLs (white color), at a fixed total layer number of ten. [133]

Sample	Stacking sequence	Tensile strength (MPa)	Elastic modulus (MPa)	Break elongation (mm/mm)
4-1		316.78 ± 0.82	24.50 ± 0.45	1.31 ± 0.03
4-2	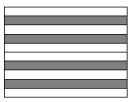	341.88 ± 4.24	25.18 ± 0.40	1.36 ± 0.02

6-1	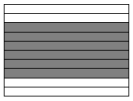	451.26 ± 14.66	36.38 ± 0.69	1.24 ± 0.01
6-2	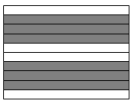	515.67 ± 10.37	39.20 ± 0.91	1.31 ± 0.02

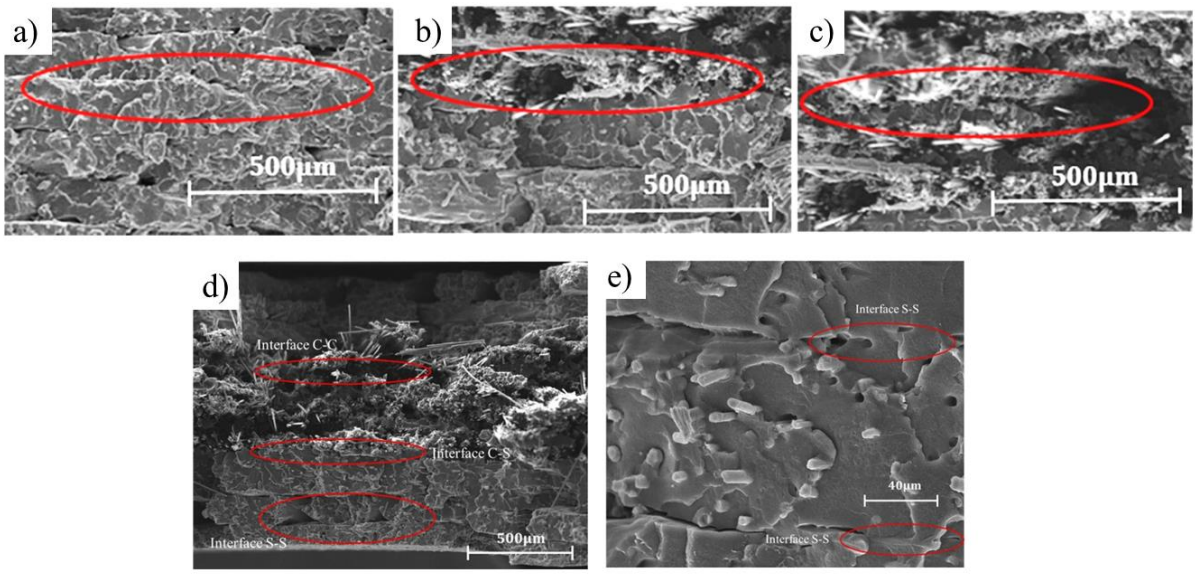

Fig. 15. SEM images for the interfaces (a) S-S, (b) C-S and (c) C-C of the printed laminated composites before mechanical testing. (d) Tensile fracture surface of the laminated composites with 4 CCFRLs in the middle. (e) Tensile fracture interfaces between SCFRLs (S-S). Here, the red circles mark the layer interfaces. Reprinted with permission from Ref. [133]

The presence of voids at the C-C and C-S interfaces was attributed to the initial gaps within the CCF towpreg. Additionally, the mobility of the melted Nylon matrix was hindered by the high content of the carbon fibers during the printing process of the CCF tows, leading to the formation of more voids. Figs. 15d and 15e show the fracture surface of the printed composite parts after tensile testing. As can be seen, delamination was observed at the C-C interfaces (Fig. 15d), while both C-S and S-S interfaces had less bonding issues. The results

suggested that the printed composite samples with the separated CCFR layers had more C-S and S-S interfaces with improved interfacial bonding and, therefore, exhibited higher mechanical performance. Additionally, these interfaces prevented stress concentrations and resulted in efficient stress transfer between the reinforcing CFs and the Nylon matrix [133]. The findings suggest that the tensile strength of the printed continuous fiber-reinforced composite with a specific fiber volume fraction can be improved by minimizing the C-C interfaces via tailoring the stacking sequence of the layers. However, although continuous fiber-reinforced composite parts printed at higher fiber volume fraction possess more C-C interfaces, they usually have better tensile strength because the strengthening effects of the reinforcing fibers are much more significant compared to weakening effects of the C-C interfaces [134].

3.3.2 Mechanical improvements of FFF printed parts by the continuous fiber-reinforced composite approach

Fig. 16 shows IEI values for tensile strength and Young's modulus of the parts printed by the continuous fiber-reinforced composite approach. As can be seen, most research work reported the improvement of the mechanical properties in longitudinal direction and no improvement data for the transverse orientation were available. The two-nozzle approach with Onyx and Nylon matrix shows the best reinforcement efficiency with IEI values of up to 29.8 times for tensile strength and 314.6 times for Young's modulus. Their achieved mechanical properties are also the highest with a tensile strength of up to 581 MPa and a Young's modulus of up to 64.5 GPa. The IEI values for both tensile strength and Young's modulus of the parts printed by the one-nozzle approach are less than 6 times and 9 times, respectively. The lower results of the one-nozzle approach are attributed to the weaker interfacial bonding between the reinforcing fibers and the polymer matrix, as well as the lower achieved fiber volume fraction. In fact, the reported volume fraction of the one-nozzle

approach is only in the range of 6.1 to 34% while the two-nozzle approach can reach a volume fraction of up to 54%. Generally, CFs provide the best reinforcement effects compared to other reinforcing fibers thanks to their high mechanical strength.

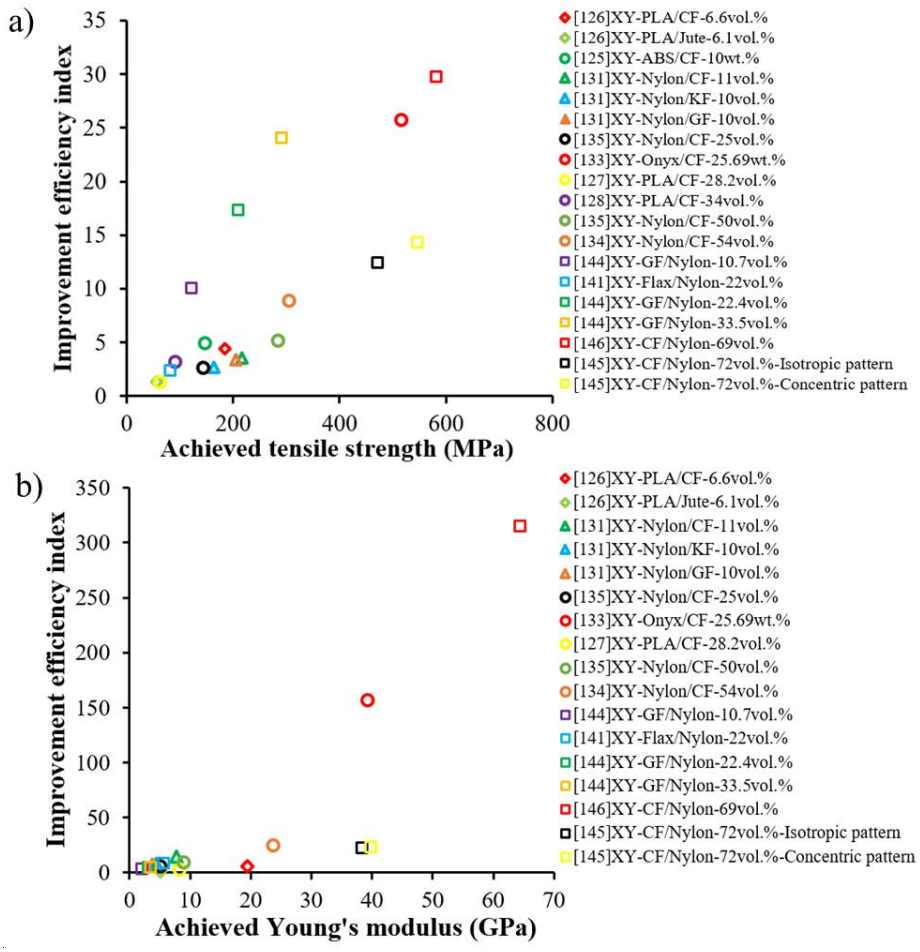

Fig. 16. Plots of (a) IEI value of tensile strength versus achieved strength and (b) IEI value of Young's modulus versus achieved Young's modulus via the continuous fiber-reinforced composite method.

4 Post-treatment methods

4.1 Approaches for post-treatment of FFF printed parts

Post-treatment is an alternative approach to improve mechanical performance of FFF printed parts. Several research studies have reported the successful enhancement in tensile

strength of the printed parts via ultrasonic welding, laser heating, annealing, and microwave heating. The underlying mechanisms for these improvements are related to the enhancement of the interfacial bonding between layers/rasters and reduction of porosity by applying different external energy sources after the printing process.

a) Ultrasonic welding

Ultrasonic plastic welding has been applied to strengthen the bonding between the deposited layers to improve the mechanical properties of the FFF printed parts. Figs. 17a and b illustrate an ultrasonic welding process and its strengthening mechanism reported by Li *et al.* [147]. In their study, a FFF printed sample was first fixed to a work surface before being contacted by an ultrasonic horn. Then, pressure and ultrasonic vibrations were applied to the sample through the horn for strengthening. Under static pressure, the ultrasonic vibration energy was transferred to the internal parts and transformed into friction energy of the internal bond of the FFF printed sample. It was then transformed into deformation and heat energy to fuse the broken raster and defects within the printed sample. After the strengthening process, the horn continued to hold the sample for a certain period to prevent warpage.

By applying the ultrasonic post-processing, Li *et al.* improved tensile strength and Young's modulus of ABS samples printed by the FFF process by up to 11.3% and 16.7%, respectively [147]. Moreover, the tensile performance of the samples showed a continuously upward trend with increasing ultrasonic strengthening time and pressure since these factors increased the amount of vibration energy input to the printed parts. Fracture surface of the tested samples in Figs. 17c and d suggested that ultrasonic welding treatment fused the inter-raster voids and strengthen the printed structures. Notably, the increase of the strengthening time and pressure was not infinite as excessive input energy damaged the sample surface in contact with the horn, leading to a cloak phenomenon or surface pasting.

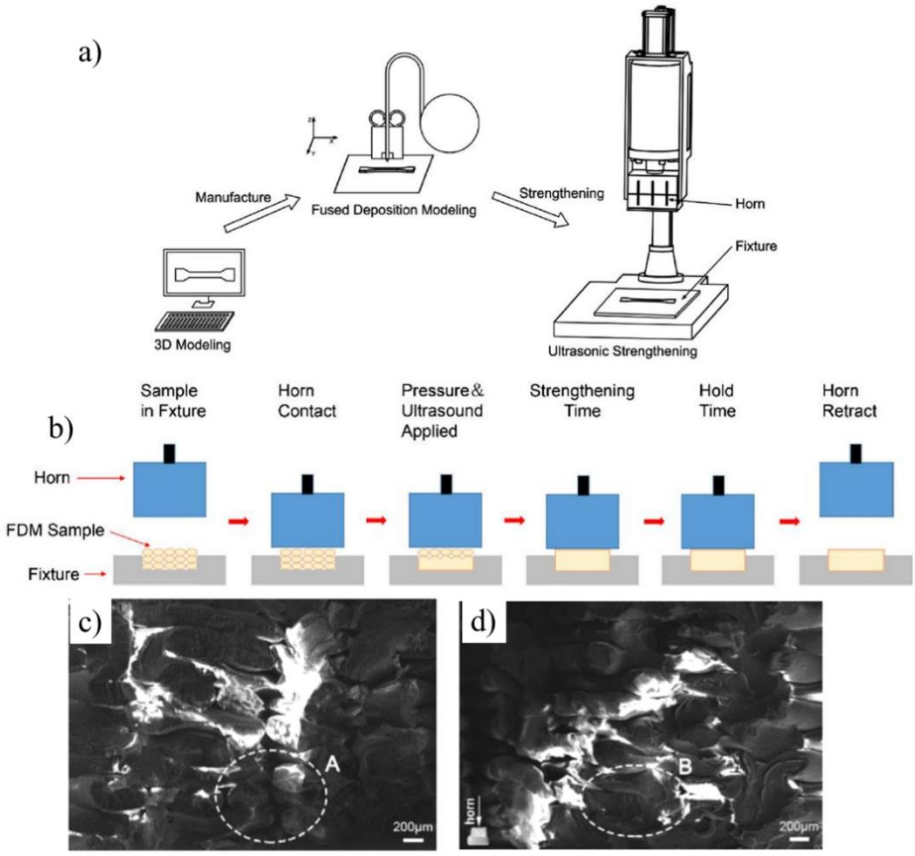

Fig. 17. Schematic illustration of (a) ultrasonic strengthening 3D printing process and (b) ultrasonic strengthening mechanism. Fracture surface of (c) untreated samples and (d) ultrasonic strengthened samples with an exposure time of 0.25s. Here, circle A marks the void region of the untreated samples and circle B marks the fused region of the ultrasonic strengthened samples. Reprinted with permission from Ref. [147]

In another study, Li *et al.* reported the positive effects of ultrasonic strengthening on mechanical properties of ABS and PLA samples printed by FFF process [46]. Specifically, the tensile strength and Young's modulus of the ABS printed samples increased by 12.94% and 16.56%, respectively, while the figures for the PLA printed parts were 22.83% and 20.62%, respectively, after the ultrasonic treatment. These improvements were attributed to the reduced spaces between the interface of the rasters and increased interfacial bonding area after the introduction of the ultrasonic strengthening. Notably, these studies only reported positive effects on mechanical properties of tensile samples with simple geometry. In fact, it

might be challenging to apply this method to complex shaped parts due to the requirement of a suitable horn geometry.

b) Laser treatment

While laser heating has been mainly used to enhance surface quality of FFF printed parts in several studies, it has also been reported that this post-treatment has positive effects on the mechanical properties of the printed parts. Chen *et al.* first reported the enhancement of up to 13.2% in tensile strength and 9.8% in Young's modulus of PLA parts printed by FFF process after polishing their surface by laser heating [47]. This was primarily due to the reduced porosity and improved surface quality of the specimens after the treatment. In the process shown in Figs. 18a and b, the laser generated heat energy onto the surface of the specimen, which broke down the polymer chains at the surface region. The material then melted and a stagnation pressure occurred on the surface of the specimen, whereby the formation of compressive force flattened the surface of the specimens and closed up the internal air gaps and defects.

The gaps and defects included gas porosity, which was formed during the shrinkage from the melt to solid state of the material during the printing process. The re-melting mechanism also introduced greater thermal adhesion between interlayers, reduced the material delamination and adjacent layer separation during tensile testing (Figs. 18c and d). Additionally, the rapid heating and cooling process during the laser polishing treatment produced cold work hardening phenomena, lowering the ductility of the PLA specimen. In their later study for heat exchanger applications, effects of the laser treatment on tensile strength of the FFF printed Al/PLA parts were evaluated [148]. The study reported an increase in tensile strength from 41.01 MPa to 54.88 MPa and Young's modulus from 776.5 MPa to 1078.4 MPa after applying laser polishing treatment. Since only the regions near the

surface of the printed parts were affected by the laser heating, this method might be mainly applicable to improve mechanical properties of thin-walled polymer parts.

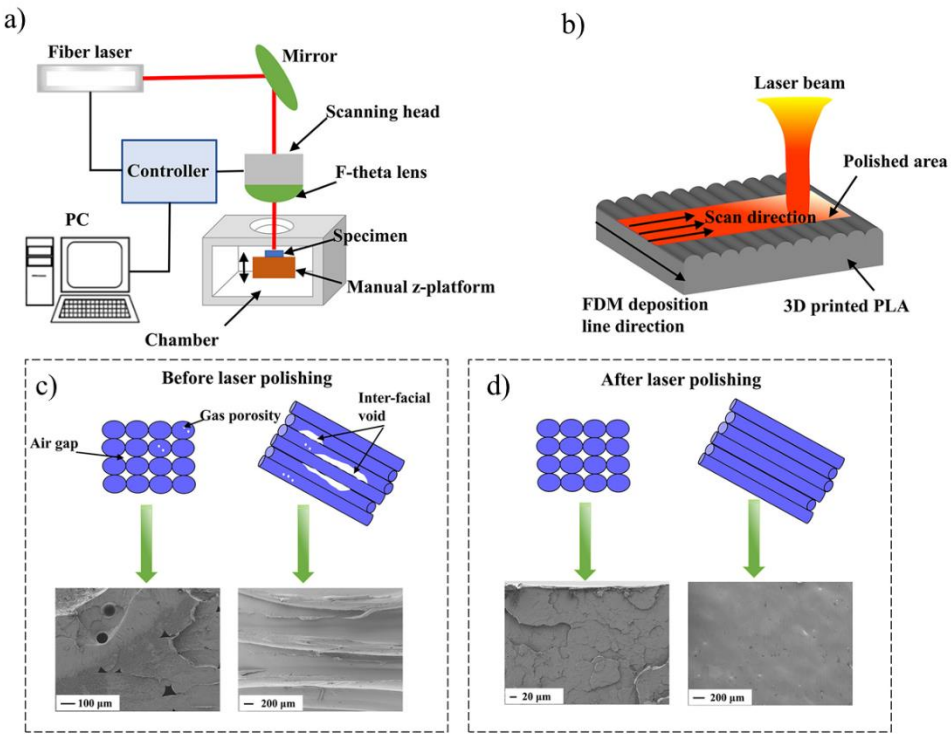

Fig. 18. Schematic illustration of (a) experimental setup for laser polishing, (b) the remelting mechanism and laser scanning direction, (c) defective printed PLA specimen, and (d) perfect printed PLA specimen. Reprinted with permission from Ref. [47]

c) Heat treatment

Similar to laser and ultrasonic strengthening, heat treatment methods such as hot pressing and annealing are also effective approaches to improve mechanical performance of FFF printed parts. Jo *et al.* studied the effects of hot pressing on mechanical strength of PLA parts printed by FFF process [149]. As shown in Fig. 19a, the printed samples were positioned at the center of a custom-designed Al mold and then covered by a top plate. The mold was then located within the center of a forced convection oven, while a uniform pressure was applied to the mold by a load cell with different weights (1.5, 9, and 19 N) located at the top plate. The whole system was subsequently heated up to 160 °C at different

heating time durations (0, 30, 60 and 120 s). Fig. 19b shows the mechanical properties of the FFF printed parts treated at different heat treatment conditions. As can be seen, the heat treatment was able to improve the tensile strength of the FFF printed samples by 5, 8, and 58% for 0.1, 0.2, and 0.3 mm thick layers. This improvement was attributed to the increased molecular diffusion and higher randomization of the PLA polymer chains across the layer interface as the interfacial tension of the adjacent rasters was lower during the heat treatment at 160 °C, leading to stronger interlayer bonding.

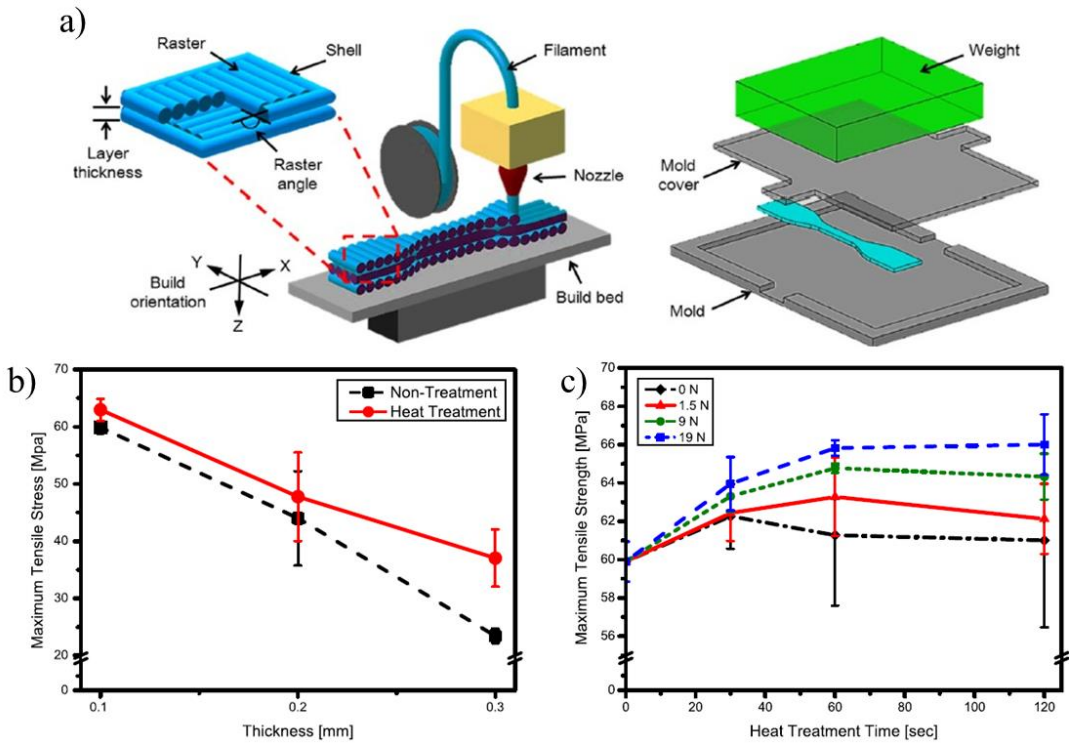

Fig. 19. (a) Schematic illustration of experimental setup for heat treatment of FFF printed PLA parts. (b) Stress-strain curve of specimens with different pressure loading during heat treatment. (c) Maximum tensile strength against heat treatment duration of the specimens with different pressure loading. Reprinted with permission from Ref. [149]

Additionally, pressure under heating and heating time also plays a crucial role in the efficiency of the heat treatment. As presented in Fig. 19c, tensile strength of the PLA parts printed at the layer thickness of 0.1 mm increased with increasing applied pressure and

heating time. Specifically, the specimens treated under the highest pressure (19 N) and longest heat treatment time (120 s) possessed the highest increase in tensile strength (10.2%) compared to the untreated samples. This was explained by the fact that high pressure improved the polymer diffusion rate, while a long heating time provided sufficient time for complete polymer diffusion between the adjacent rasters. These results were supported by the disappearance of the interface between the rasters observed in their cross-sections at higher applied pressure and heating time. Consequently, voids at the interfaces were minimized, leading to optimized stress transfer and higher mechanical performance of the post-treated samples. In a later study, Rane *et al.* applied similar approach to reduce the void content at the layer interfaces and improved the transverse strength of FFF printed ABS parts by 89%, reaching 34.22 MPa [48]. The main issue of the hot pressing method is its high cost due to the requirement of compression molds, especially for complex shaped parts.

In another approach, Bhandari *et al.* studied effects of annealing on tensile strength of FFF printed CF/PLA and CF/PETG parts in transverse direction [150]. In the study, the PETG composite samples were annealed at 120 °C, which was above their glass transition temperature, whereas the CF/PLA parts were annealed at 90 °C and 120 °C to evaluate the effect of cold crystallization during the annealing process. The annealing time for all samples was varied between 30 and 480 min. The results showed that the tensile strength and Young's modulus of the printed CF/PETG parts annealed at 120 °C increased from 12.4 to 32.4 MPa and from 1.4 to 2.3 GPa, respectively. Similarly, the CF/PLA parts annealed at 90 °C achieved a tensile strength of 30.8 MPa and Young's modulus of 3.3 GPa, corresponding to an increase of 93% and 44%, respectively. It was found that annealing enhanced interlayer diffusion of polymer molecules at the layer interfaces, resulting in increased entanglements and consequently superior mechanical performance. Additionally, the annealing treatment was reported to have a positive effect on tensile strength of polymer blends [151] and liquid-

crystal-polymers [152]. Compared to hot pressing, the annealing method is more cost-effective as no molds are required.

d) Microwave heating

Sweeney *et al.* reported the use of locally induced radio frequency (LIRF) welding method to improve the interface bonding between layers of PLA coated with CNTs in FFF printing process [28]. In this study, a solution of PLA, chloroform, and CNTs was used to coat a 14 μm thick PLA/CNT layer on the surface of commercial PLA filaments. These coated filaments were then used for FFF printing of macroscopic structures with CNTs localized only at the raster interfaces. Since CNTs absorbed microwave radiation and efficiently converted it into heat, the CNT loaded interfaces of the FFF printed parts could be selectively heated once they were exposed to microwave irradiation, leading to improved local polymer mobility and diffusion across the raster interface (Fig. 20). Consequently, the fracture strength of the parts treated with microwave heating increased by 275% compared to that of the parts printed by the neat PLA.

The results were evidenced by the large necked zones along the tear path with significant plastic deformation observed in the fracture surface of the LIRF welded parts. More importantly, the fracture strength of the LIRF-welded parts was even higher than that of the neat hot-pressed parts, which was probably due to the local increased crystallinity of the polymer interface or the reinforcement effects of the CNTs at the interface. The positive effects of microwave heating on the tensile properties of the FFF printed parts were later reported by Wang *et al.* [153]. In their study, a thin layer of SiC/PLA composite film was coated on neat PLA filaments before FFF printing and microwave heating. Since SiC could absorb microwave energy efficiently, the SiC loaded interfaces were selectively heated when exposed to microwave irradiation, leading to an increase of 51% and 18.7% in tensile strength in longitudinal and transverse directions of the printed parts, respectively.

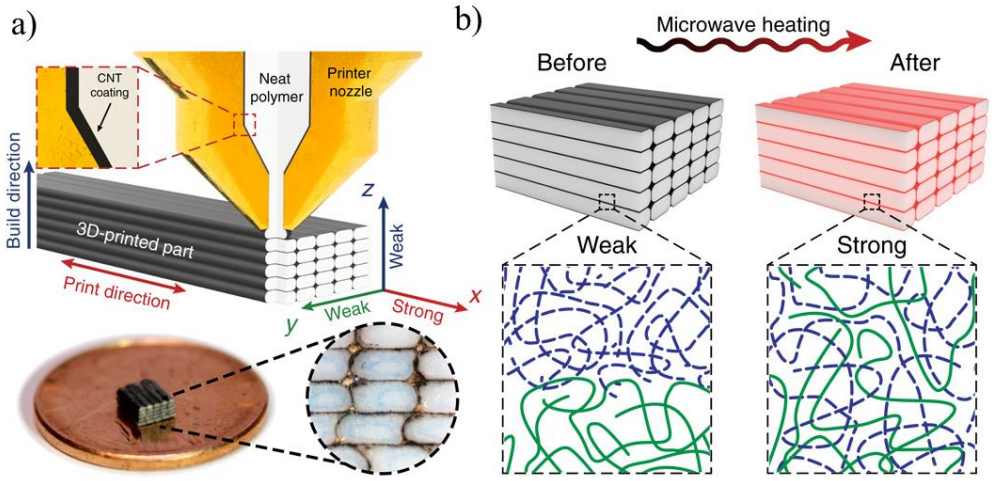

Fig. 20. Schematic of (a) FFF process of PLA filament with a CNT-rich layer; the resulting 3D-printed part contains RF-sensitive nanofillers localized at the interface. (b) Mechanism of locally heated interface under microwave irradiation for improved polymer diffusion. Reprinted with permission from Ref. [28]

e) Z-pinning

Z-pinning is a common method to improve mechanical properties of laminated composite by inserting high-strength pins or rods in Z direction. Todoroki *et al.* first applied z-pinning method to enhance Z-strength of FFF printed continuous carbon fiber (CCF)/ Nylon composite parts [154]. In their study, a printed Z-pin bar made of CCF/Nylon composite with a dimension of 5.8 × 1.9 × 100 mm was inserted into a rectangular hole (5.8 × 1.9 mm) of a printed part for strength improvement, as shown in Fig. 21a. As the bar was electrically conductive, it could be heated by applying a large electric current to enable fusion bonding at the interface between the bar and the printed composite part (self-heating). The reinforcing bar had 25 mm margins at both ends which were acted as electrodes for current application (Fig. 21b). The X-ray computed tomography (CT) cross-sections of the printed samples shown in Figs 21c and d suggested a strong interfacial bond formed between the reinforcing bar and the printed sample. Due to the reinforcement effects of the Z-pin, the tensile strength and Young's modulus of the printed CCF/Nylon parts reached 41.9 MPa and

8.94 GPa, corresponding to an improvement of 726% and 273%, respectively. Notably, the mechanical properties of the treated parts in longitudinal direction were not reported in this study. After the fusion bonding process, the in-plane strength was expected to be lower than that of parts printed by conventional FFF process due to formation of voids at the interface between the reinforcing bar and the printed part, as shown in Fig. 21d.

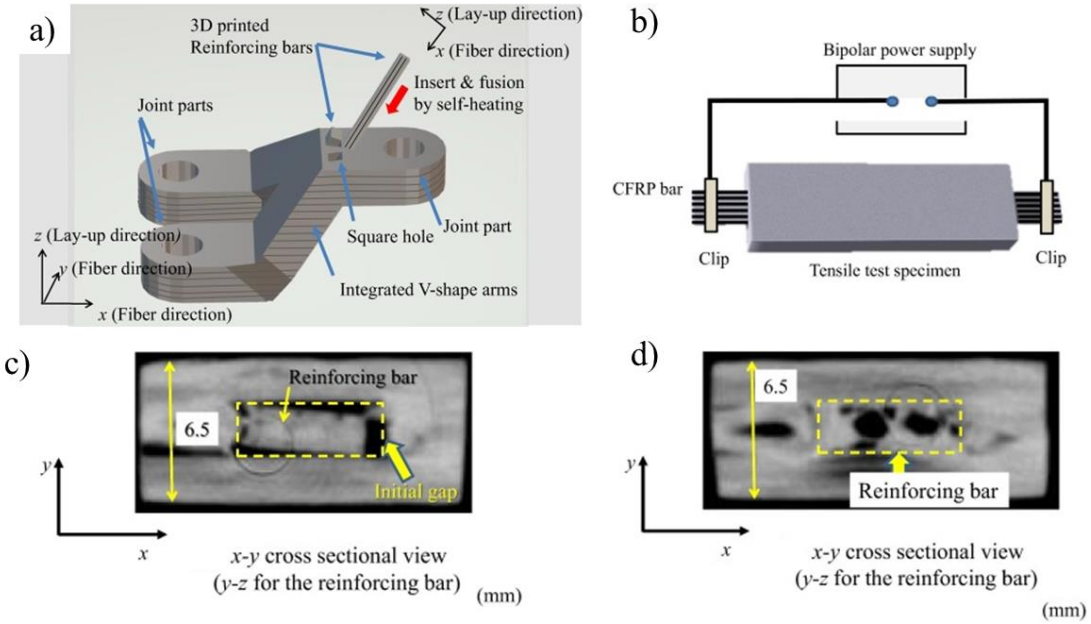

Fig. 21. Schematic of (a) Z-pinning process for Z-strength improvement and (b) resistive heating process for fusion bonding at the interface between the bar and the printed composite part. X-Ray CT images of tensile specimen before (c) and after the fusion process (d). Here, the yellow boxes mark the hole region. Reprinted with permission from Ref. [154]

4.2 Mechanical improvements of FFF printed parts by post-treatment approach

Fig. 22 shows IEI values and achieved mechanical properties of the post-treated FFF printed parts. As can be seen, the post-treatment methods can effectively improve the mechanical properties in transverse direction with IEI values for tensile strength and Young's modulus ranging between 1.13 to 8.26 and 1.14 to 3.73 times, respectively. Z-pinning is the most effective method with an IEI value of 8.26 times for Z-strength and 3.73 times for Z-Young's modulus. Regarding the mechanical performance in longitudinal direction, all

reported IEI values achieved for both tensile and Young's modulus are below 1.4 times. The microwave heating and laser polishing reported the highest IEI values for longitudinal strength (1.34 times). Although the efficiency in longitudinal strength of the hot press method is quite low, its IEI value for the Young's modulus is among the highest (1.39 times).

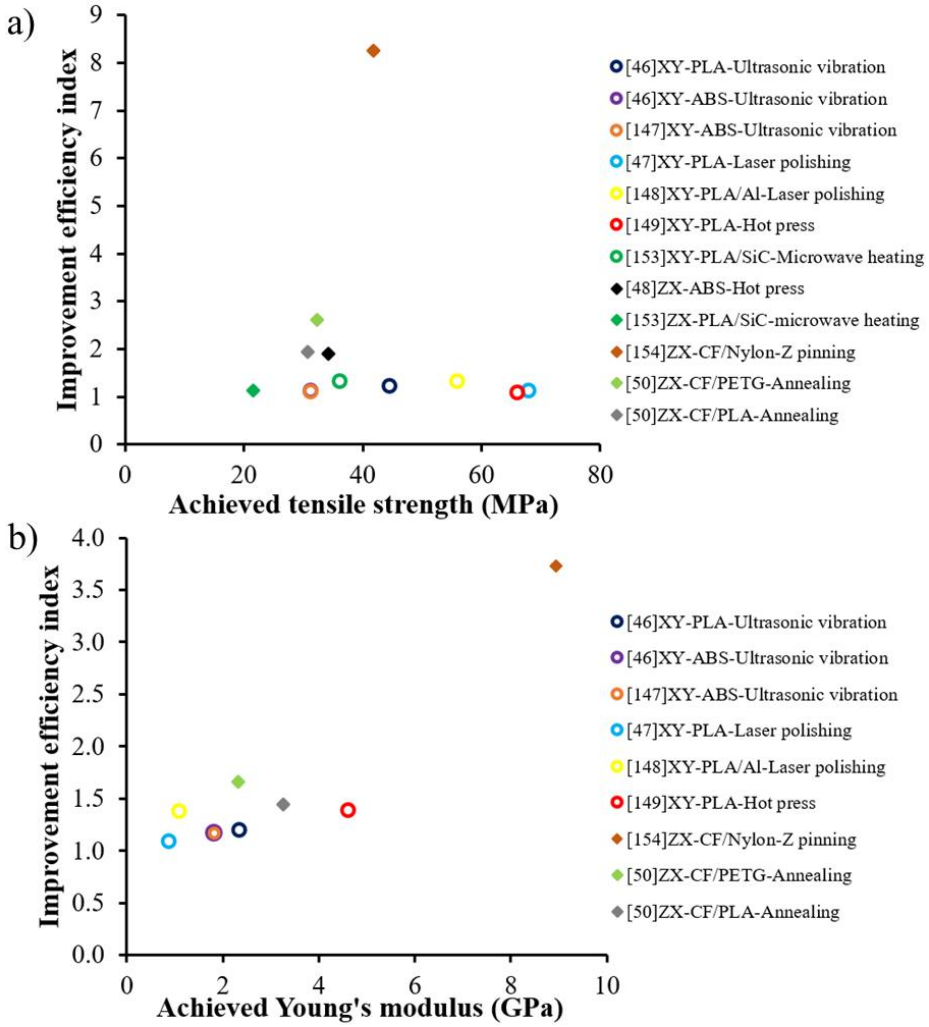

Fig. 22. Plots of (a) IEI value of tensile strength versus achieved strength and (b) IEI value of Young's modulus versus achieved Young's modulus via post-treatment method.

5. Process modification of FFF

Based on the review in the earlier sections, it is obvious that significant mechanical improvements can be achieved by material modifications and post-processing steps. However, these approaches usually involve additional steps before and/or after the printing

process, leading to increased cost and longer processing time. To address these issues, researchers have studied FFF process modifications to achieve similar or improved results during in-situ processing. Some of the reported FFF process modifications include material and extruder modifications for localized cross-linking or heating, printing in sub-ambient atmospheric pressure, and installation of pressing/ vibrating equipment for enhanced filament contact. In this section, these various techniques are presented and discussed.

5.1 Approaches for modification of FFF printing process

a) Cross-linking of layer interfaces by ultraviolet (UV) irradiation

The improvement of anisotropic properties of FFF printed parts through the introduction of localized UV-induced bonding was reported by Levenhagen *et al.* [155]. In this study, 35k PLA LMW-SuSAs such as dimethacrylated PLA (PLADM) or trimethacrylated PLA (PLATM) and 2,2-dimethoxy-2-phenylacetophenone (DMPA) photoinitiator were added to commercial PLA to enable UV-induced cross-linking between the printed layers. In the setup shown in Fig. 23a, a UV light-emitting diode was attached to the print head of a FFF printer for in-situ cross-linking of the deposited rasters during the printing process. It was found that the PLATM and PLDM blends printed with the in-situ UV irradiation exhibited a significant improvement of up to 140 and 200% in transverse tensile strength, reaching 35 and 45 MPa, respectively.

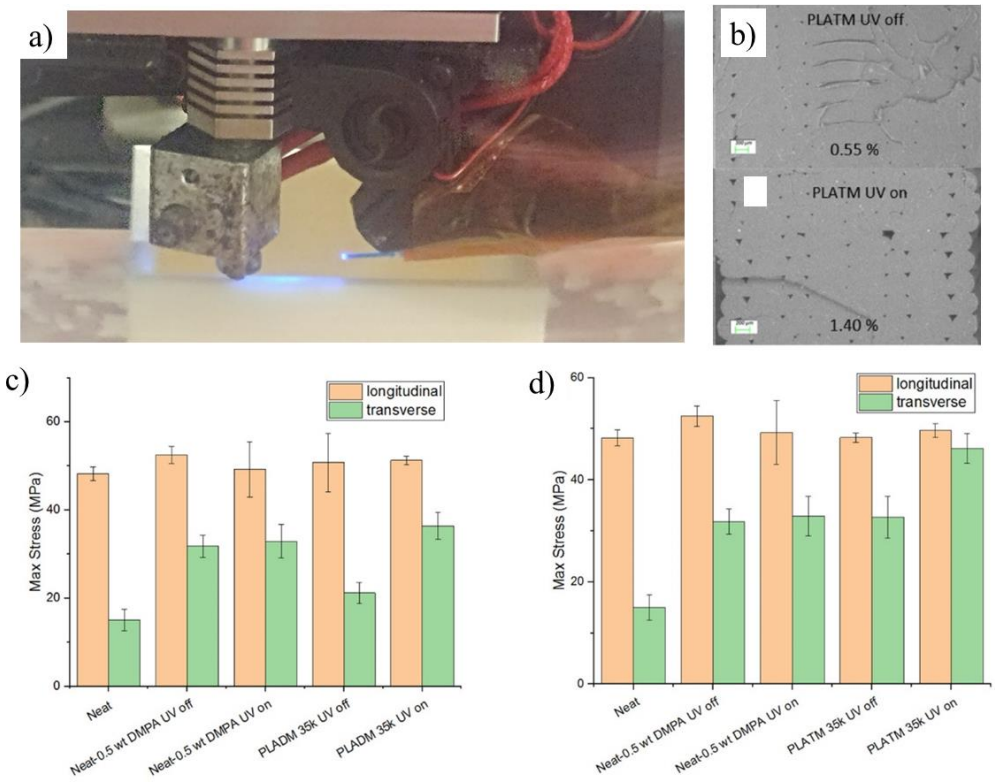

Fig. 23. (a) In situ UV irradiation setup. (b) Cross-section of PLA printed parts with 0.5 wt % DMPA and 3 mol % PLATM UV off and on. Tensile strength of (c) PLADM series at 3 mol % loading with 0.5 wt % DMPA loading and (d) PLATM series at 3 mol % loading with 0.5 wt % DMPA loading. Reprinted with permission from Ref. [155]

This impressive result stemmed from the superior interlayer bonding between filament layers as the LMW species more readily diffused and entangled in the layer interface, while strong covalent bonds were formed across those interfaces via UV-induced cross-linking reactions between the methacrylate groups. However, larger interfilamentous voids observed in the internal structure of the UV-irradiated samples (Fig. 23b) suggested that the UV reaction occurred rapidly to covalently bond the layers, therefore hindering the interlayer diffusion. Notably, the UV intensity was tailored to control the formation rate of the cross-links between the printed layers. The formation rate needed to be balanced such that the reaction was slow enough to not hinder interlayer diffusion but fast enough to generate sufficient covalent bonds between the layers in the final samples. In general, the samples

treated with the LMW-SuSAs and in-situ UV irradiation exhibited more isotropic mechanical properties along the longitudinal and transverse directions as seen in Figs. 23c and d.

b) Localized laser pre-deposition heating

In another approach, Ravi *et al.* reported an in-process localized laser pre-deposition heating method to enhance the interlayer bonding in the FFF printing process [50]. In their experimental setup shown in Fig. 24a, an 802 nm laser was used as a laser source to locally preheat the underlying printed layers before the deposition of ABS extrudates. It was found that the nozzle printing speed had to be higher than 4 mm/s to avoid defects formed by excessive evaporation of the materials at high intensity regions. The benefit of the localized pre-heating method was the ability to locally heat up the underlying area above polymer's glass transition temperature, hence improving interlayer bonding without impacting the part dimension stability. Consequently, the inter-layer bond strength of the printed parts increased by 50%. In their later study, the localized laser pre-deposition heating method was employed to enhance the tensile strength of FFF printed ULTEM parts [156]. After the process improvement method was applied, a 178% improvement in Z-strength of the printed samples was achieved, suggesting the potential of this in-process method to address the anisotropic mechanical property issue of the FFF process.

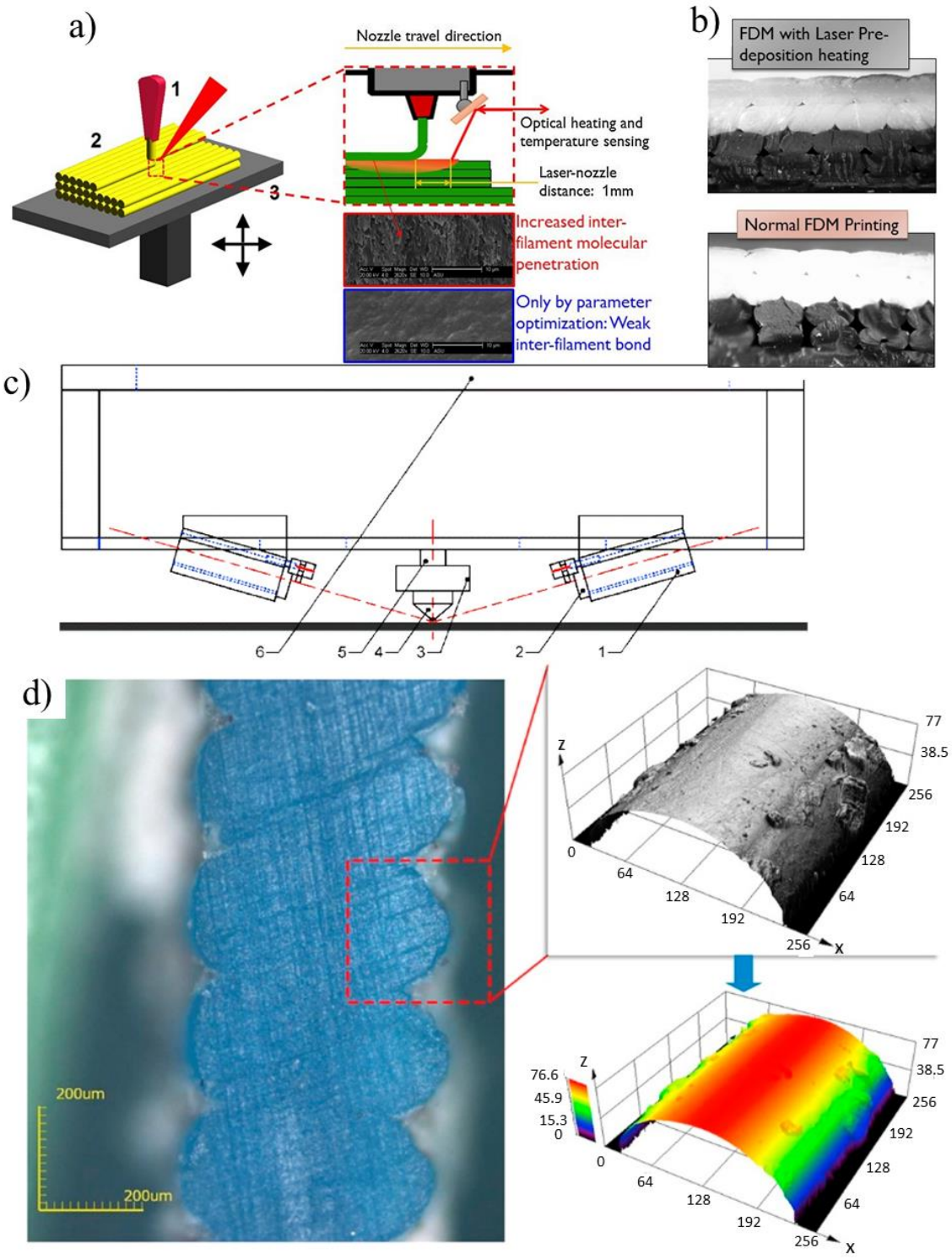

Fig. 24. (a) Concept illustration of laser local pre-deposition heating approach in FFF process. (b) Optical micrograph of freeze-fractured printed samples with and without in-process laser pre-deposition heating. Reprinted with permission from Ref. [50]. (c) Schematic

diagram of the improved FFF process with laser-assisted heating device: (1) fixed device, (2) infrared fiber laser, (3) heater, (4) nozzle, (5) liquifier, (6) support. (d) Cross-section profiles of the thin-walled parts by the single-layer-multiple-paths forming and pre- and post-laser-assisted heating. Reprinted with permission from Ref. [157].

In another study, Jun *et al.* reported an improvement of up to 195% in tensile strength of large-size thin-walled ABS parts printed by FFF process equipped with laser-assisted heating devices [157]. In their modified printer shown in Fig. 24c, 2 laser sources were attached to the printer for local heating of the region below the printing nozzle during the printing process of thin-walled samples with a wall thickness of 0.4 mm. Based on the relative position relationships between the spreading direction of the polymer melt and the laser beams, two cases of laser-assisted heating were investigated: lateral heating (perpendicular to the spreading direction) and pre- and post-heating (parallel to the spreading direction). It was found that the laser-assisted heating approach provided local input of energy to increase the temperature of the printing areas, reduced the viscosity of the ABS melt, and improved the interlayer diffusion of the printed polymer layers (Fig. 24d). Additionally, the lateral laser-assisted heating was more efficient to enhance the interlayer bonding strength compared to the pre- and post-heating since its lateral laser beam was able to cover more printing areas with higher energy intensities.

c) Interface welding by dielectric barrier discharge

Sweeney *et al.* reported an in-process welding method by heating the CNT-loaded interfaces using dielectric barrier discharge (DBD) plasma to enhance interlayer bonding of FFF printed parts [29]. In their modified FFF process shown in Fig. 25a, a concentric DBD plasma applicator disc was mounted around the nozzle of a FFF printer for in-process welding of polyamide (PA) filaments coated with CNTs. As the CNTs had a significant heating response to electric fields, the thermoplastic CNT-loaded interfaces were uniformly

heated by the DBD plasma without physical contact between the printed material and the high-voltage electrode. Specifically, a DBD between the FFF deposited layer and the bottom of the applicator disc was excited by a high voltage kilohertz radio frequency (RF) signal during the printing process (Fig. 25b), while the nozzle served as the ground electrode. Consequently, the fringing electric field generated a hemitoroidal heating zone both behind and ahead of the deposited layer (Fig. 25c). In fact, the current passing through the printed parts produced rapid resistive heating of the CNTs and, therefore, welded the layer interfaces.

The temperature profile of the DBD-heated PA part also indicated that they achieved a surface temperature of 180 °C, which was much higher than the glass transition temperature (~40 °C) and near the melting temperature of the neat PA (189 °C). Therefore, the time at the required temperature for the formation of a complete bond between successive layers was substantial, leading to an increase of 31% in the Z-strength of the printed parts. More interestingly, this strength was comparable to that of the injection molded samples, as shown in Fig. 25d, indicating great potential for this approach.

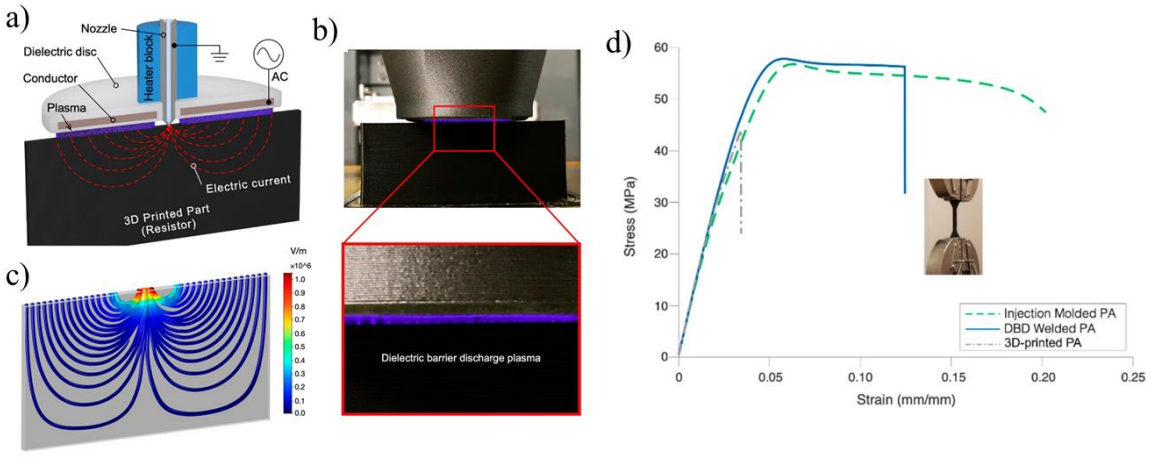

Fig. 25. (a) Cutaway diagram of the dielectric barrier discharge welding hardware and electric field interactions with a 3D-printed plaque. (b) Photo of the DBD plasma discharge interacting with a printed PA6,66 sample. (c) COMSOL simulation of the electric field lines between the DBD applicator disc, the sample, and the printer nozzle. (d) Stress−strain curve

of a DBD treated mechanical PA6,66 specimen, a 3D-printed control specimen, and an injection-molded specimen. Reprinted with permission from Ref. [29]

d) Pressing/vibration assisted printing

Besides the use of localized energy, mechanical means such as rollers and vibration-assisted setup are also effective methods to improve layer adhesion and mechanical properties of FFF printed parts [158-160]. Majit *et al.* reported the use of a mechanical pressing fixture attached to the nozzle of a FFF printer to reduce the porosity and, hence, improve the tensile strength of ABS printed parts [158]. In their study, two chrome steel rollers with a diameter of 1 cm and a width of 0.8 cm were attached to the heat sink of the FFF printhead and moved along the direction of the nozzle. The position of the rollers was fixed at the same level of the nozzle, so that they could move and press on the deposited material concurrently during the printing process. It was found that the porosity of the coupons printed by the integrated pressing process reduced by 8%, while the deposited filaments were flattened and packed against each other. Consequently, the tensile strength of the integrated pressing coupons increased by approximately 28 %, reaching 38.34 MPa.

In another approach, Keles *et al.* used a vibration motor attached to the nozzle of a FFF printer to provide vibration effects during the printing process of short CF/ABS printed parts [159]. In their modified process, the extrusion nozzle was vibrated by a 12 V vibration motor with an offset weight of 30 g. The vibration amplitude and frequency were approximately 0.15 mm and 375 Hz, respectively. The modified process showed a decrease in the inter-raster porosity and pore size. Specifically, the total porosity of the printed parts reduced from 13 % to 10 %. This was attributed to the physical pushing of the nozzle caused by the vibration effects, resulting in the spreading of the printed melt toward the deposited materials. Therefore, the tensile strength of the printed parts increased by 13%, reaching 27.3 MPa. One concern of this method was the reduction in dimensional precision and surface

quality of the printed parts due to the vibrations. In fact, the parts printed by this modified process had slightly larger dimensions and rougher surfaces with a wavy raster observed at their side surface. To address these issues, different methods such as dimensional compensation, process optimization, and post-treatments can be employed to improve the dimensional accuracy and surface quality of the printed parts.

e) FFF printing in vacuum/inert atmosphere

Several studies have been conducted to investigate the effects of the FFF printing in sub-ambient atmospheric pressure and inert environment on the mechanical performance of the printed parts. Maidin *et al.* reported the use of FFF printing process in a low pressure vacuum atmosphere to address the issue of incomplete interfacial bonding of the printed parts [49]. In this study, an acrylic chamber was used to seal a FFF printer and provide vacuum atmosphere for the printing process. Since there was a reduction of air molecules in low pressure vacuum environment, the heat loss due to convection of air during the FFF printing process reduced. This allowed the extruded polymer melt to be maintained at high temperature for a longer period of time for complete bonding between the printed layers. Consequently, the transverse tensile strength of the ABS specimens printed at 18 inHg increased by up to 12.83% compared to those printed in atmospheric pressure. However, a disadvantage of this approach is that the heat trapped in the vacuum chamber affects the electronic components of the FFF printer. Therefore, the system needed to be redesigned to avoid component damage.

In another approach, Mazlan *et al.* reported the use of an inert gas-assisted FFF process to print ABS materials for higher tensile strength and larger surface roughness [162]. A mild steel and a chrome-coated chamber were used to seal a FFF printer in a N_2 environment. It was found that the inert atmosphere reduced the degradation of the polymer caused by the presence of oxygen at high temperature, such as oxidation and thermal

degradation during the FFF process. Consequently, the surface roughness of the printed parts reduced from 11 to 6.5 µm, while their tensile strength increased by 28%.

f) Integrated pre- and post- heating

Ravoori *et. al.* reported a nozzle-integrated pre- and post- heating approach to improve the mechanical properties of PLA parts printed by the FFF process [163]. In their modified process, a 30-mm-long Aluminum heater block with an additional pre-heater element was integrated to the printhead to obtain the pre/post-heating configuration, as shown in Fig. 26a. Two different preheater blocks with their bottom surface located at 0.6 and 1.6 mm above the nozzle tip were built. The gap between the nozzle tip and the printing surface was fixed at 0.35 mm to control the gap between the bottom surface of the two preheater blocks and the printing surface at 0.95 mm and 1.95 mm, respectively. The Al block acted as a preheater when the nozzle moved in one printing direction and became a post-heater for the reverse direction. By bolting together two separately machined Al blocks, a pre- and post-heater could also be fabricated for simultaneous heating effects.

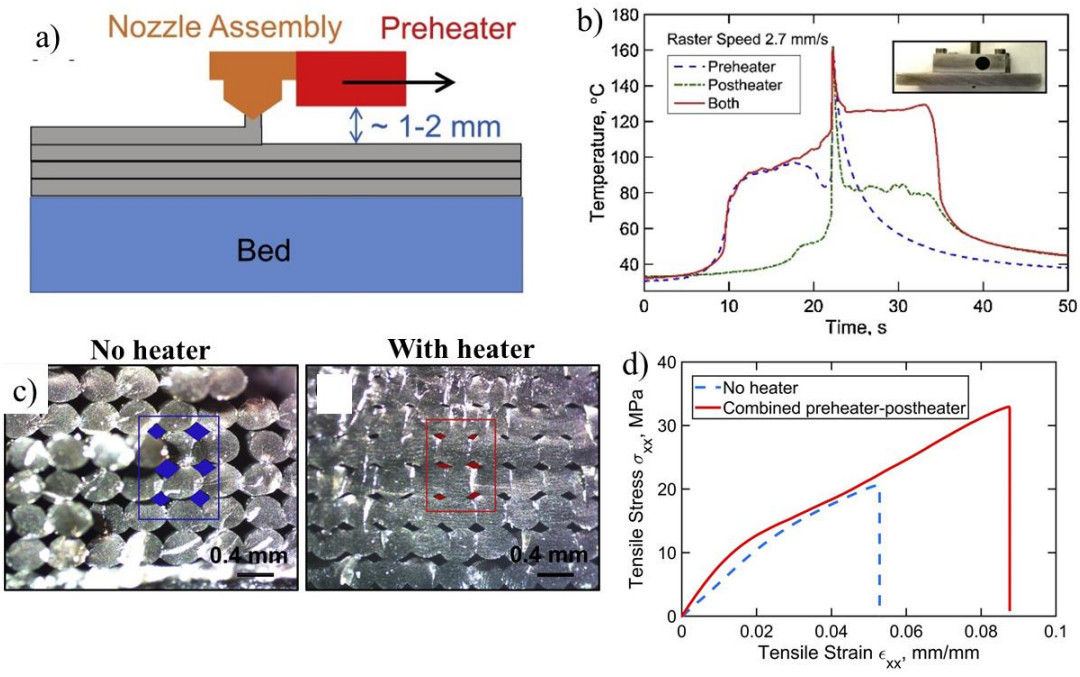

Fig. 26. (a) Schematic of nozzle-integrated hot surface based preheating. (b) Temperature plots comparing the impact of preheater and postheater configurations with a case where both preheater and postheater are used. (c) Cross-section images of printed samples with and without pre/post heating. Here, blue and red rectangular boxes mark selected regions to determine void content fraction of samples printed without and with pre/post heating, respectively. (d) Stress-strain curve of samples printed at 3600 mm/min scan speed with and without preheater-postheater heating. Reprinted with permission from Ref. [163]

It was found that a lower heater-to-base gap led to a higher temperature rise due to increased radiation and conduction heat transfer between the two surfaces. In addition, a lower printing speed was found to prolong elevated temperature of the deposited areas since they were exposed to the hot preheater surface at a longer period of time during the printing process. Moreover, the combination of pre- and post-heater configuration resulted in a significant increase in temperature at the deposited areas (Fig. 26b). Specifically, at the printing speed of 60 mm/s and heater-to-base gap of 0.95 mm, the pre- and post- heater configuration increased the filament-to-filament necking with less pores observed in their internal structure, as shown in Fig. 26c. Consequently, the tensile strength and toughness of the PLA parts printed from pre- and post-heater configuration increased by 60% and 165%, respectively (Fig. 26d) [163]. The result indicated that the pre-and post-heating approach supplied sufficient thermal energy to the deposited layers for effective interfacial bonding and improved mechanical performance.

5.2 Mechanical improvements of FFF printed parts by process modification approach

Fig. 27 presents the IEI values and the achieved mechanical properties of the FFF printed parts via the process modification method. As can be seen, the IEI values of the tensile strength and Young's modulus produced by the process modification are in the range of 1.02 to 3 and 1.08 to 2 times, respectively. Interestingly, higher achievements in the Z-

strength of the FFF printed parts are observed as this approach mainly focuses on the enhancement of the interlayer diffusion. Among the reported methods, the cross-linking of layer interfaces by UV radiation and the laser preheating show the highest efficiency with IEI values of up to 3 times, although the tensile strength achieved by the cross-linking of layer interface is much higher than that of the laser preheating. Despite the low IEI value, plasma heating achieved the highest Z-strength, which is comparable to properties fabricated by conventional processing methods.

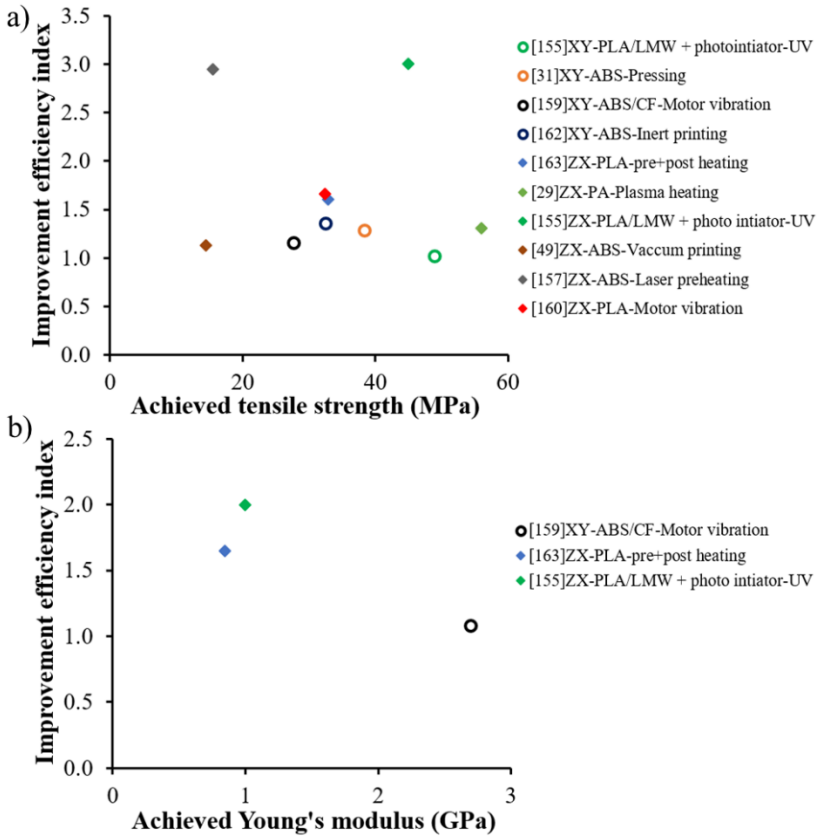

Fig. 27. Plots of (a) IEI value of tensile strength versus achieved strength and (b) IEI value of Young's modulus versus achieved Young's modulus via process modification method.

6. Advantages and challenges of the process improvement approaches for mechanical improvements of FFF printed parts

Fig. 28 summarises the IEI values and achieved mechanical properties of parts printed by FFF processing in longitudinal direction for the different process improvement approaches

discussed in the earlier sections. As can be seen, both material blend and post-treatment approaches result in the lowest IEI values for XY-strength (below 1.5 times) and XY-modulus (below 2 times). Although the discontinuous filler-reinforced composite and process modification methods possess comparable IEI values for XY-strength (~ 1 - 4 times), the IEI values and achieved data for XY-Young's modulus of the discontinuous filler-reinforced composite method are in a much higher range. Specifically, its IEI values and achieved XY-Young's modulus values range from 1 to 9 times and 0.5 to 9 GPa, respectively, while the figures for the process modification method range only from 1 to 2.3 times and 1 to 2 GPa, respectively. This is attributed to the reinforcement effects of the fillers used in the discontinuous filler-reinforced composite method.

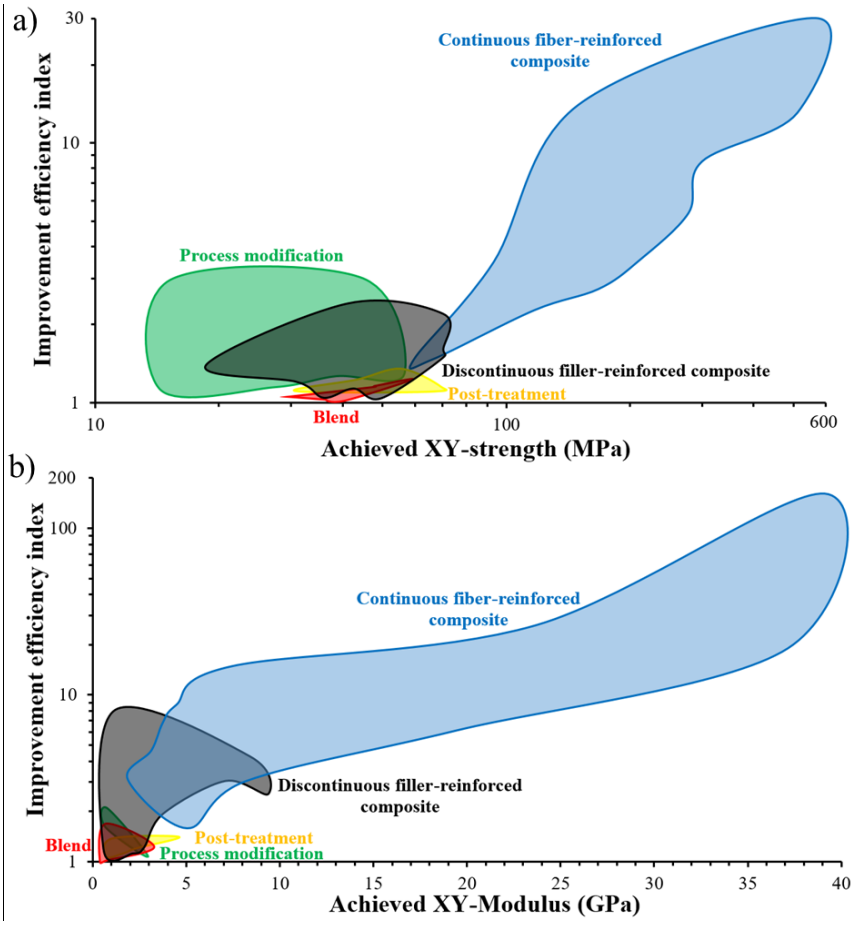

Fig. 28. Plots of (a) IEI value of XY-strength versus achieved XY-strength and (b) IEI value of XY-Young's modulus versus achieved XY-Young's modulus via blend, discontinuous

filler-reinforced composite, continuous fiber-reinforced composite, process modification, and post-treatment methods.

Notably, all aforementioned approaches only possess IEI values for tensile strength and Young's modulus in longitudinal direction less than 4 and 10 times, respectively, corresponding to achieved XY-strength of below 100 MPa and achieved XY-Young's modulus properties of below 10 GPa. This performance is only comparable to that of the neat polymer parts produced by conventional methods such as injection molding. However, the continuous fiber-reinforced composite method offers the best improvement in mechanical performance in longitudinal direction with IEI values of up to 30 times for tensile strength and 315 times for Young's modulus. This is mainly due to the outstanding mechanical properties of their continuous reinforcing fibers. More importantly, its achieved XY-strength and XY-Young's modulus are up to 581 MPa and 65 GPa, respectively, which are attractive for structural applications.

Fig. 29 summarises the IEI values and achieved mechanical properties of parts printed by FFF process in transverse direction for different process improvement approaches outlined in the earlier sections. As can be seen, the material blend, post-treatment, and process modification methods are highly effective to improve the tensile strength in the Z-direction of the FFF printed parts. Their IEI values and achieved Z-strength are in the range from 1 to 8 times and from 8 to 45 MPa, respectively. The discontinuous filler-reinforced composite method, however, has the lowest IEI values ranges (below 2 times), although its achieved Z-strength is comparable to that of the other methods. Regarding the Young's modulus in Z-direction, the post-treatment and process modification methods obtain high IEI values (~ 1.5 - 4 times), while the improvement ranges for both blend and discontinuous filler-reinforced composite methods are below 1.5 times. The Z-modulus achieved by the post-treatment method is the highest and in the range from 2.32 to 8.94 GPa. Notably, there are no reported

data for mechanical performance in transverse direction of the parts fabricated via the continuous fiber-reinforced composite method in literature.

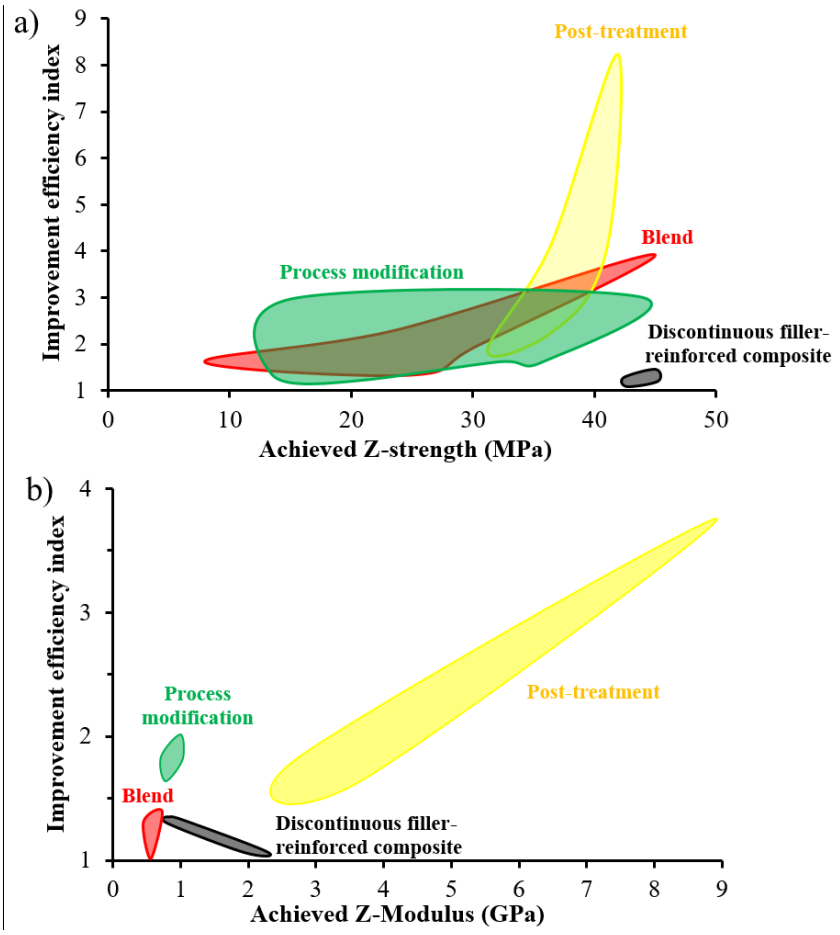

Fig. 29. Plots of (a) IEI value of Z-strength versus achieved Z-strength and (b) IEI value of Z-Young's modulus versus achieved Z-Young's modulus via blend, discontinuous filler-reinforced composite, process modification, and post-treatment methods.

Overall, the continuous fiber-reinforced composite is the most effective method to enhance the tensile strength of the FFF printed parts in longitudinal direction. However, the long reinforcing fibers are costly, which could limit the cost efficiency of the FFF method. Besides, the anisotropy issues are expected to be more severe in composite parts printed by this approach due to the unidirectional orientation of the reinforcing fibers deposited along longitudinal direction only although no data on 3D printed specimens have been reported in literature so far. The material blend, post-treatment, and process modification are the main

approaches to improve the mechanical performance in Z-direction and address the anisotropic issue of the FFF printed parts, but their effectiveness on the tensile strength in longitudinal direction is insignificant.

All material modification approaches usually require significant effort to fabricate new feedstock filaments and optimize their respective FFF printing process parameters, resulting in an increase in cost and processing time. Additionally, as this approach is material-dependent, this process needs to be repeated for each new feedstock material based on different application requirements. The post-treatment and process modification methods may also experience an increase in cost and processing time due to the requirements of additional complex equipment needs and/or additional post-processing steps. However, as these are process-based approaches, the process parameters can be tailored to adapt quickly to different feedstock materials. In other words, post-treatment and process modification methods are considered more cost-effective for processing a wide range of feedstock materials.

Due to the facile processability, most reported studies on the process improvement approaches employ commodity plastics such as PLA and ABS for the FFF printing. Additionally, there are a limited number of matrix polymers available for the continuous fiber-reinforced composite method. Markforged printers are the most commonly used FFF systems to fabricate continuous fiber-reinforced composites based on the large number of reported studies in literature. However, the printers used in most reported studies are limited to only processing Nylon and short CF/Nylon composite as the matrix materials. The other in-house printers reported in literature generally work with commodity plastics such as PLA and ABS with limited critical applications. In practice, many end-use applications require the processing of different engineering and high-performance polymers. For example, ULTEM^{TM} is the only accredited polymer used in FFF process for aerospace application to-date due to

stringent flammability requirements, while medical applications require the usage of biopolymers such as PEEK due to biocompatibility constraints. Accordingly, there are limited studies investigating the effects of the process improvement approaches on the tensile properties of the printed parts made from different amorphous and semicrystalline polymers. Since these materials have differing polymer dynamics with temperature, a fundamental understanding of their behaviours during the application of different process improvement approaches is crucial to 3D printing of high-performance polymer parts for a wide range of end-use applications.

7. Conclusion and future direction

This paper presents a comprehensive review of research studies investigating process improvement methods for enhanced mechanical strength of parts printed by FFF processing, including material blend, discontinuous filler-reinforced composite, continuous fiber-reinforced composite, post-treatment, and process modification. The advantages, challenges, and mechanical performance of the parts produced by each approach have been identified and evaluated. By comparing the improvement efficiency and achieved mechanical properties of the parts printed by FFF process with the different approaches, this review paper offers guidance to enable evaluation of the impact of the various proposed process improvement methods to fabricate FFF printed parts for high performance applications. In addition, new research results can quickly be added for benchmarking purposes for future evaluations.

For tensile strength, the material blend, post-treatment, and process modification methods have great potential to address the weak Z-direction property issue. In particular, these methods can be employed to offer an achieved Z-strength of more than 40 MPa with IEI values of up to 8 times. Moreover, the high mechanical performance in longitudinal direction of parts printed by the continuous fiber-reinforced composite method is attractive for many end-use applications, since it is the only option to achieve a longitudinal strength of

more than 100 MPa. Regarding the Young's modulus in longitudinal direction, both continuous fiber-reinforced and discontinuous filler-reinforced composite methods can offer satisfactory improvement efficiencies. Specifically, the former method can fabricate polymer parts with a Young's modulus of up to 9 GPa, while the achieved figures for the latter can be as high as 65 GPa. However, post-treatment is the only method that can fabricate parts with a Young's modulus in Z-direction of more than 2.3 GPa.

It is foreseen that future research will focus on improving the mechanical performance of the parts printed by FFF process to further address the remaining issues of the current methods, while exploring additional new potential approaches to achieve better improvement efficiency. Additional studies about process improvement approaches for different engineering and high-performance polymers will need to be conducted to meet a wider range of industrial applications. Mechanical deficiency in Z-strength is still one of the most crucial challenges in the FFF process that remains to be resolved, especially for the continuous fiber-reinforced composite approach. Available technologies developed for conventional fabrication methods of continuous fiber-reinforced polymer composites, such as 3D weaving and through-thickness stitching, can offer further inspirations for process development.

Lastly, the integration of high performance polymers such as ULTEM^{TM}, PEEK, and PVDF as matrix materials in the continuous fiber-reinforced composite approach for high-value applications is considered to be one of the main focus areas for future FFF developments. With the recent introduction of new Markforged printers, research studies on FFF printing of continuous fiber-reinforced ULTEM composite are expected to increase significantly in the near future. Besides, hybrid approaches with the combination of at least two process improvement approaches could be a promising solution to enhance the mechanical performance of the FFF printed parts. The blend and/or composite approaches can be combined with all possible process modification methods such as pre-and post-heating

or vibration assisted printing to improve the printing process and the printed structures. More importantly, the resulting parts can be post-treated to further increase their mechanical performance for different end-use applications.

CRediT authorship contribution statement

The authors declare the following roles: **Thang Q. Tran**: Conceptualization, Supervision, Writing – original draft, review & editing. **Feng Lin Ng**: Resources, Project administration, Writing – original draft, review & editing. **Justin Tan Yu Kai**: Writing – original draft. **Stefanie Feih:** Conceptualization, Writing - review & editing. **Mui Ling Sharon Nai**: Writing - review & editing.

Declaration of Competing Interest

The authors declare that they have no known competing financial interests or personal relationships that could have appeared to influence the work reported in this paper.

Acknowledgments

We thank SIMTech for financial support of this paper. Professor Stefanie Feih acknowledges support from the School of Engineering and Built Environment, Griffith University, Queensland, Australia. Her affiliation has changed since completion of the work, and she can be contacted at s.feih@griffith.edu.au.

References

[1] U.M. Dilberoglu, B. Gharehpapagh, U. Yaman, M. Dolen, The Role of Additive Manufacturing in the Era of Industry 4.0, Procedia Manuf. 11 (2017) 545-554.

[2] S.A.M. Tofail, E.P. Koumoulos, A. Bandyopadhyay, S. Bose, L. O'Donoghue, C. Charitidis, Additive manufacturing: scientific and technological challenges, market uptake and opportunities, Mater. Today 21(1) (2018) 22-37.

[3] S.H. Ahn, K.T. Lee, H.J. Kim, R. Wu, J.S. Kim, S.H. Song, Smart soft composite: An integrated 3D soft morphing structure using bend-twist coupling of anisotropic materials, Int. J. Precis. Eng. Manuf. 13(4) (2012) 631-634.

[4] N.A. Ahmed, J.R. Page, Manufacture of an Unmanned Aerial Vehicle (UAV) for advanced project design using 3D printing technology, Appl. Mech. Mater. 397–400 (2013) 970–980.

[5] S.V. Murphy, A. Atala, 3D bioprinting of tissues and organs, Nat. Biotechnol. 32(8) (2014) 773-785.

[6] S.J. Paulsen, J.S. Miller, Tissue vascularization through 3D printing: Will technology bring us flow?, Dev. Dyn. 244(5) (2015) 629-640.

[7] J.W. Stansbury, M.J. Idacavage, 3D printing with polymers: Challenges among expanding options and opportunities, Dent. Mater. 32(1) (2016) 54-64.

[8] B. Berman, 3-D printing: The new industrial revolution, Bus. Horiz. 55(2) (2012) 155-162.

[9] C.R. Garcia, R.C. Rumpf, H.H. Tsang, J.H. Barton, Effects of extreme surface roughness on 3D printed horn antenna, Electron. Lett. 49(12) (2013) 734-736.

[10] C.R. Garcia, R.C. Rumpf, H.H. Tsang, J.H. Barton, Effects of extreme surface roughness on 3D printed horn antenna, Electron. Lett. 49(12) (2013) 734-736.

[11] Q. Zhang, C. Li, The Roles of Traditional Chinese Medicine: Shen-Fu Injection on the Postresuscitation Care Bundle, Evid. Based Complement. Alternat. Med. 2013 (2013) 319092.

[12] W. Serrano-Garcia, W.A.D.M. Jayathilaka, A. Chinnappan, T.Q. Tran, C. Baskar, S.W. Thomas, S. Ramakrishna, Nanocomposites for electronic applications that can be embedded for textiles and wearables, Sci. China Technol. Sci. 62(6) (2019) 895-902.

[13] W.A.D.M. Jayathilaka, A. Chinnappan, D. Ji, R. Ghosh, T.Q. Tran, S. Ramakrishna, Facile and Scalable Electrospun Nanofiber-Based Alternative Current Electroluminescence (ACEL) Device, ACS Appl. Electron. Mater. 3(1) (2021) 267-276.

[14] F. Hajializadeh, A. Ince, Finite element–based numerical modeling framework for additive manufacturing process, Mater. Des. Process. Commun. 1(1) (2019) e28.

[15] A. Gholamipour-Shirazi, M.A. Kamlow, I.T. Norton, T. Mills, How to Formulate for Structure and Texture via Medium of Additive Manufacturing-A Review, Foods 9(4) (2020) 497.

[16] N. Grimmelsmann, M. Kreuziger, M. Korger, H. Meissner, A. Ehrmann, Adhesion of 3D printed material on textile substrates, Rapid Prototyp. J. 24(1) (2018) 166-170.

[17] R. Melnikova, A. Ehrmann, K. Finsterbusch, 3D printing of textile-based structures by Fused Deposition Modelling (FDM) with different polymer materials, IOP Conf. Ser.: Mater. Sci. Eng. 62 (2014) 012018.

[18] D. Schmelzeisen, H. Koch, C. Pastore, T. Gries, 4D Textiles: Hybrid Textile Structures that Can Change Structural Form with Time by 3D Printing, in: Y. Kyosev, B. Mahltig, A. Schwarz-Pfeiffer (Eds.), Narrow and Smart Textiles, Springer International Publishing, Cham, 2018, pp. 189-201.

[19] S. Lepak-Kuc, P. Taborowska, T.Q. Tran, H.M. Duong, T. Gizewski, M. Jakubowska, J. Patmore, A. Lekawa-Raus, Washable, colored and textured, carbon nanotube textile yarns, Carbon 172 (2021) 334-344.

[20] I. Hager, A. Golonka, R. Putanowicz, 3D Printing of Buildings and Building Components as the Future of Sustainable Construction?, Procedia Eng. 151 (2016) 292-299.

[21] I. Perkins, M. Skitmore, Three-dimensional printing in the construction industry: A review, Int. J. Constr. Manag. 15(1) (2015) 1-9.

[22] P. Wu, J. Wang, X. Wang, A critical review of the use of 3-D printing in the construction industry, Autom. Constr. 68 (2016) 21-31.

[23] F. Bos, R. Wolfs, Z. Ahmed, T. Salet, Additive manufacturing of concrete in construction: potentials and challenges of 3D concrete printing, Virtual Phys. Prototyp. 11(3) (2016) 209-225.

[24] E.O. Olakanmi, Selective laser sintering/melting (SLS/SLM) of pure Al, Al–Mg, and Al–Si powders: Effect of processing conditions and powder properties, J. Mater. Process. Technol. 213(8) (2013) 1387-1405.

[25] T. Pereira, J. Potgieter, J.V. Kennedy, A fundamental study of 3D printing testing methods for the development of new quality management strategies, 2017 24th International Conference on Mechatronics and Machine Vision in Practice (M2VIP), 2017, pp. 1-6.

[26] S.C. Ligon, R. Liska, J. Stampfl, M. Gurr, R. Mülhaupt, Polymers for 3D Printing and Customized Additive Manufacturing, Chem. Rev. 117(15) (2017) 10212-10290.

[27] S.C. Daminabo, S. Goel, S.A. Grammatikos, H.Y. Nezhad, V.K. Thakur, Fused deposition modeling-based additive manufacturing (3D printing): techniques for polymer material systems, Mater. Today Chem. 16 (2020) 100248.

[28] C.B. Sweeney, B.A. Lackey, M.J. Pospisil, T.C. Achee, V.K. Hicks, A.G. Moran, B.R. Teipel, M.A. Saed, M.J. Green, Welding of 3D-printed carbon nanotube–polymer composites by locally induced microwave heating, Sci. Adv. 3(6) (2017) e1700262.

[29] C.B. Sweeney, M.L. Burnette, M.J. Pospisil, S.A. Shah, M. Anas, B.R. Teipel, B.S. Zahner, D. Staack, M.J. Green, Dielectric Barrier Discharge Applicator for Heating Carbon Nanotube-Loaded Interfaces and Enhancing 3D-Printed Bond Strength, Nano Lett. 20(4) (2020) 2310-2315.

[30] X. Gao, S. Qi, X. Kuang, Y. Su, J. Li, D. Wang, Fused filament fabrication of polymer materials: A review of interlayer bond, Addit. Manuf. 37 (2021) 101658.

[31] M. Harris, J. Potgieter, R. Archer, K.J.M. Arif, Effect of Material and Process Specific Factors on the Strength of Printed Parts in Fused Filament Fabrication: A Review of Recent Developments, Materials 12 (2019) 1664.

[32] E. Cuan-Urquizo, E. Barocio, V. Tejada-Ortigoza, R.B. Pipes, C.A. Rodriguez, A. Roman-Flores, Characterization of the mechanical properties of FFF structures and materials: A review on the experimental, computational and theoretical approaches, Materials 12(6) (2019) 895.

[33] D. Popescu, A. Zapciu, C. Amza, F. Baciu, R. Marinescu, FDM process parameters influence over the mechanical properties of polymer specimens: A review, Polym. Test. 69 (2018) 157-166.

[34] I.J. Solomon, P. Sevvel, J. Gunasekaran, A review on the various processing parameters in FDM, Mater. Today: Proc. 37 (2021) 509-514.

[35] A. Dey, N. Yodo, A systematic survey of FDM process parameter optimization and their influence on part characteristics, J. Manuf. Mater. Process. 3(3) (2019) 64.

[36] M. Lalegani Dezaki, M.K.A. Mohd Ariffin, S. Hatami, An overview of fused deposition modelling (FDM): research, development and process optimisation, Rapid Prototyp. J. 27(3) (2021) 562-582.

[37] M. Kam, A. Ipekci, O. Sengul, Investigation of the effect of FDM process parameters on mechanical properties of 3D printed PA12 samples using Taguchi method, J. Thermoplast. Compos. Mater. (2021) 08927057211006459.

[38] J. Jiang, J. Lou, G. Hu, Effect of support on printed properties in fused deposition modelling processes, Virtual Phys. Prototyp. 14(4) (2019) 308-315.

[39] J. Jiang, Y. Ma, Path Planning Strategies to Optimize Accuracy, Quality, Build Time and Material Use in Additive Manufacturing: A Review, Micromachines 11(7) (2020) 633.

[40] C.Y. Jingchao Jiang, Xun Xu, Yongsheng Ma, Jikai Liu, Achieving better connections between deposited lines in additive manufacturing via machine learning, Math. Biosci. Eng. 17(4) (2020) 3382-3394.

[41] X. Wang, M. Jiang, Z. Zhou, J. Gou, D. Hui, 3D printing of polymer matrix composites: A review and prospective, Compos. Part B Eng. 110 (2017) 442-458.

[42] K. Yang, J.C. Grant, P. Lamey, A. Joshi-Imre, B.R. Lund, R.A. Smaldone, W. Voit, Diels–Alder Reversible Thermoset 3D Printing: Isotropic Thermoset Polymers via Fused Filament Fabrication, Adv. Funct. Mater. 27(24) (2017) 1700318.

[43] N.P. Levenhagen, M.D. Dadmun, Interlayer diffusion of surface segregating additives to improve the isotropy of fused deposition modeling products, Polymer 152 (2018) 35-41.

[44] E.H. Tumer, H.Y. Erbil, Extrusion-Based 3D Printing Applications of PLA Composites: A Review, Coatings 11(4) (2021) 390.

[45] H.G. Zhang, T.L. Huang, Q.X. Jiang, L.L. He, A. Bismarck, Q.X. Hu, Recent progress of 3D printed continuous fiber reinforced polymer composites based on fused deposition modeling: a review, J. Mater. Sci. 56(23) (2021) 12999-13022.

[46] G.W. Li, J. Zhao, W.Z. Wu, J.L. Jiang, B.F. Wang, H. Jiang, J.Y.H. Fuh, Effect of Ultrasonic Vibration on Mechanical Properties of 3D Printing Non-Crystalline and Semi-Crystalline Polymers, Materials 11(5) (2018) 826.

[47] L. Chen, X. Zhang, S. Gan, Effects of laser polishing on surface quality and mechanical properties of PLA parts built by fused deposition modeling, J. Appl. Polym. Sci. 137(3) (2020) 48288.

[48] R. Rane, A. Kulkarni, H. Prajapati, R. Taylor, A. Jain, V. Chen, Post-Process Effects of Isothermal Annealing and Initially Applied Static Uniaxial Loading on the Ultimate Tensile Strength of Fused Filament Fabrication Parts, Materials 13(2) (2020) 352.

[49] S. Maidin, J.H.U. Wong, A.S. Mohamed, S.B. Mohamed, R.A. Rashid, Z.I. Rizman, Vacuum Fused Deposition Modelling System to Improve Tensile Strength of 3D Printed Parts, J. Fundam. Appl. Sci. 9 (2017) 839-853.

[50] A.K. Ravi, A. Deshpande, K.H. Hsu, An in-process laser localized pre-deposition heating approach to inter-layer bond strengthening in extrusion based polymer additive manufacturing, J. Manuf. Process. 24 (2016) 179-185.

[51] Z. Liu, Y. Wang, B. Wu, C. Cui, Y. Guo, C. Yan, A critical review of fused deposition modeling 3D printing technology in manufacturing polylactic acid parts, Int. J. Adv. Manuf. Technol. 102(9) (2019) 2877-2889.

[52] O.S. Carneiro, A.F. Silva, R. Gomes, Fused deposition modeling with polypropylene, Mater. Des. 83 (2015) 768-776.

[53] M. Spoerk, C. Holzer, J. Gonzalez-Gutierrez, Material extrusion-based additive manufacturing of polypropylene: A review on how to improve dimensional inaccuracy and warpage, S. Appl. Polym. Sci. 137(12) (2020) 48545.

[54] A.R. Zanjanijam, I. Major, J.G. Lyons, U. Lafont, D.M. Devine, Fused Filament Fabrication of PEEK: A Review of Process-Structure-Property Relationships, Polymers 12(8) (2020) 1665.

[55] P.K. Penumakala, J. Santo, A. Thomas, A critical review on the fused deposition modeling of thermoplastic polymer composites, Compos. Part B Eng. 201 (2020) 108336.

[56] S.J. Park, J.E. Lee, J. Park, N.-K. Lee, Y. Son, S.-H. Park, High-temperature 3D printing of polyetheretherketone products: Perspective on industrial manufacturing applications of super engineering plastics, Mater. Des. 211 (2021) 110163.

[57] A.C. Abbott, G.P. Tandon, R.L. Bradford, H. Koerner, J.W. Baur, Process-structure-property effects on ABS bond strength in fused filament fabrication, Addit. Manuf. 19 (2018) 29-38.

[58] M. Sharma, V. Sharma, P. Kala, Optimization of process variables to improve the mechanical properties of FDM structures, J. Phys. Conf. Ser. 1240 (2019) 012061.

[59] B. Huang, S. Meng, H. He, Y. Jia, Y. Xu, H. Huang, Study of processing parameters in fused deposition modeling based on mechanical properties of acrylonitrile-butadiene-styrene filament, Polym. Eng. Sci. 59(1) (2019) 120-128.

[60] H.K. Dave, N.H. Patadiya, A.R. Prajapati, S.R. Rajpurohit, Effect of infill pattern and infill density at varying part orientation on tensile properties of fused deposition modeling-printed poly-lactic acid part, Proc. Inst. Mech. Eng. Part C J. Mech. Eng. Sci. 235(10) (2021) 1811-1827.

[61] B. Shaqour, M. Abuabiah, S. Abdel-Fattah, A. Juaidi, R. Abdallah, W. Abuzaina, M. Qarout, B. Verleije, P. Cos, Gaining a better understanding of the extrusion process in fused filament fabrication 3D printing: a review, Int. J. Adv. Manuf. Technol. 114(5) (2021) 1279-1291.

[62] A.W. Gebisa, H.G. Lemu, Influence of 3D Printing FDM Process Parameters on Tensile Property of ULTEM 9085, Procedia Manuf. 30 (2019) 331-338.

[63] D. Croccolo, M. De Agostinis, G. Olmi, Experimental characterization and analytical modelling of the mechanical behaviour of fused deposition processed parts made of ABS-M30, Comput. Mater. Sci. 79 (2013) 506-518.

[64] N. Kumar, P.K. Jain, P. Tandon, P.M. Pandey, The effect of process parameters on tensile behavior of 3D printed flexible parts of ethylene vinyl acetate (EVA), J. Manuf. Process. 35 (2018) 317-326.

[65] A. Lanzotti, M. Grasso, G. Staiano, M. Martorelli, The impact of process parameters on mechanical properties of parts fabricated in PLA with an open-source 3-D printer, Rapid Prototyp. J. 21(5) (2015) 604-617.

[66] A.K. Sood, R.K. Ohdar, S.S. Mahapatra, Parametric appraisal of mechanical property of fused deposition modelling processed parts, Mater. Des. 31(1) (2010) 287-295.

[67] T.J. Gordelier, P.R. Thies, L. Turner, L. Johanning, Optimising the FDM additive manufacturing process to achieve maximum tensile strength: a state-of-the-art review, Rapid Prototyp. J. 25(6) (2019) 953-971.

[68] J. Triyono, H. Sukanto, R.M. Saputra, D.F. Smaradhana, The effect of nozzle hole diameter of 3D printing on porosity and tensile strength parts using polylactic acid material, Open Eng. 10(1) (2020) 762-768.

[69] R. Anitha, S. Arunachalam, P. Radhakrishnan, Critical parameters influencing the quality of prototypes in fused deposition modelling, J. Mater. Process. Technol. 118(1) (2001) 385-388.

[70] O. Es-Said, J. Foyos, R. Noorani, M. Mendelson, R. Marloth, B.J.M. Pregger, M. Processes, Effect of Layer Orientation on Mechanical Properties of Rapid Prototyped Samples, Mater. Manuf. Process. 15 (2000) 107-122.

[71] H. Rezayat, W. Zhou, A. Siriruk, D. Penumadu, S.S. Babu, Structure–mechanical property relationship in fused deposition modelling, Mater. Sci. Technol. 31(8) (2015) 895-903.

[72] F. Rayegani, G.C. Onwubolu, Fused deposition modelling (FDM) process parameter prediction and optimization using group method for data handling (GMDH) and differential evolution (DE), Int. J. Adv. Manuf. Technol. 73(1) (2014) 509-519.

[73] J. Bonada, M.M. Pastor, I. Buj-Corral, Influence of Infill Pattern on the Elastic Mechanical Properties of Fused Filament Fabrication (FFF) Parts through Experimental Tests and Numerical Analyses, Materials 14(18) (2021) 5459.

[74] M. Lalegani Dezaki, M.K.A.M. Ariffin, A. Serjouei, A. Zolfagharian, S. Hatami, M. Bodaghi, Influence of Infill Patterns Generated by CAD and FDM 3D Printer on Surface Roughness and Tensile Strength Properties, Appl. Sci. 11(16) (2021) 7272.

[75] Y. Song, Y. Li, W. Song, K. Yee, K.Y. Lee, V.L. Tagarielli, Measurements of the mechanical response of unidirectional 3D-printed PLA, Mater. Des. 123 (2017) 154-164.

[76] X. Tian, T. Liu, C. Yang, Q. Wang, D. Li, Interface and performance of 3D printed continuous carbon fiber reinforced PLA composites, Compos. Part A Appl. Sci. Manuf. 88 (2016) 198-205.

[77] B. Brenken, E. Barocio, A. Favaloro, V. Kunc, R.B. Pipes, Fused filament fabrication of fiber-reinforced polymers: A review, Addit. Manuf. 21 (2018) 1-16.

[78] J. Cantrell, S. Rohde, D. Damiani, R. Gurnani, L. DiSandro, J. Anton, A. Young, A. Jerez, D. Steinbach, C. Kroese, P. Ifju, Experimental characterization of the mechanical properties of 3D printed ABS and polycarbonate parts, Springer International Publishing, Cham, 2017, pp. 89-105.

[79] R. Walter, K. Friedrich, M. Gurka, Characterization of mechanical properties of additively manufactured polymers and composites, AIP Conf. Proc. 1981(1) (2018) 020033.

[80] W.C. Smith, R.W. Dean, Structural characteristics of fused deposition modeling polycarbonate material, Polym. Test. 32(8) (2013) 1306-1312.

[81] C.C. Kuo, J.Y. Chen, Y.H. Chang, Optimization of Process Parameters for Fabricating Polylactic Acid Filaments Using Design of Experiments Approach, Polymers 13(8) (2021) 1222.

[82] H. Gonabadi, A. Yadav, S.J. Bull, The effect of processing parameters on the mechanical characteristics of PLA produced by a 3D FFF printer, Int. J. Adv. Manuf. Technol. 111(3) (2020) 695-709.

[83] G.A. Appuhamillage, J.C. Reagan, S. Khorsandi, J.R. Davidson, W. Voit, R.A. Smaldone, 3D printed remendable polylactic acid blends with uniform mechanical strength enabled by a dynamic Diels–Alder reaction, Polym. Chem. 8(13) (2017) 2087-2092.

[84] J.R. Davidson, G.A. Appuhamillage, C.M. Thompson, W. Voit, R.A. Smaldone, Design Paradigm Utilizing Reversible Diels–Alder Reactions to Enhance the Mechanical Properties of 3D Printed Materials, ACS Appl. Mater. Interfaces 8(26) (2016) 16961-16966.

[85] F. Peng, H. Jiang, A. Woods, P. Joo, E.J. Amis, N.S. Zacharia, B.D. Vogt, 3D Printing with Core–Shell Filaments Containing High or Low Density Polyethylene Shells, ACS Appl. Polym. Mater. 1(2) (2019) 275-285.

[86] Y.B. Tao, J.J. Shao, P. Li, S.Q. Shi, Application of a Thermoplastic Polyurethane/Polylactic Acid Composite Filament for 3D-printed Personalized Orthosis, Mater. Tehnol. 53(1) (2019) 71-76.

[87] H. Rupp, W.H. Binder, 3D Printing of Core–Shell Capsule Composites for Post-Reactive and Damage Sensing Applications, Adv. Mater. Technol. 5(11) (2020) 2000509.

[88] D.O. Kazmer, C.M. Grosskopf, D. Rondeau, V. Venoor, Design and Evaluation of General Purpose, Barrier, and Multichannel Plasticating Extrusion Screws, Polym. Eng. Sci. 60(4) (2020) 752-764.

[89] J.-R. Ai, F. Peng, P. Joo, B.D. Vogt, Enhanced Dimensional Accuracy of Material Extrusion 3D-Printed Plastics through Filament Architecture, ACS Appl. Polym. Mater. 3(5) (2021) 2518-2528.

[90] A. Sover, V. Ermolai, A.M. Raichur, R. Ciobanu, M. Aradoaei, N. Lucanu, Feasibility of Producing Core-Shell Filaments through Fused Filament Fabrication, Polymers 13(23) (2021) 4253.

[91] H. Narei, M. Fatehifar, A.H. Malt, J. Bissell, M. Souri, M. Nasr Esfahani, M. Jabbari, Numerical Simulation of a Core-Shell Polymer Strand in Material Extrusion Additive Manufacturing, Polymers 13(3) (2021) 476.

[92] D.O. Kazmer, Nozzles, hot ends, and methods of their use, U.S. Patent Application No. 17/103,339.

[93] F. Peng, Z. Zhao, X. Xia, M. Cakmak, B.D. Vogt, Enhanced Impact Resistance of Three-Dimensional-Printed Parts with Structured Filaments, ACS Appl. Mater. Interfaces 10(18) (2018) 16087-16094.

[94] D. Rasselet, A.-S. Caro-Bretelle, A. Taguet, J.-M. Lopez-Cuesta, Reactive Compatibilization of PLA/PA11 Blends and Their Application in Additive Manufacturing, Materials 12(3) (2019) 485.

[95] W. Niu, Z. Zhang, Q. Chen, P.-F. Cao, R.C. Advincula, Highly Recyclable, Mechanically Isotropic and Healable 3D-Printed Elastomers via Polyurea Vitrimers, ACS Mater. Lett. 3(8) (2021) 1095-1103.

[96] N.P. Levenhagen, M.D. Dadmun, Improving Interlayer Adhesion in 3D Printing with Surface Segregating Additives: Improving the Isotropy of Acrylonitrile–Butadiene–Styrene Parts, ACS Appl. Polym. Mater. 1(4) (2019) 876-884.

[97] A.S. de León, A. Domínguez-Calvo, S.I. Molina, Materials with enhanced adhesive properties based on acrylonitrile-butadiene-styrene (ABS)/thermoplastic polyurethane (TPU) blends for fused filament fabrication (FFF), Mater. Des. 182 (2019) 108044.

[98] B.E. Yamamoto, A.Z. Trimble, B. Minei, M.N.G. Nejhad, Development of multifunctional nanocomposites with 3-D printing additive manufacturing and low graphene loading, J. Thermoplast. Compos. Mater. 32(3) (2019) 383-408.

[99] S. Rostom, M.D. Dadmun, Improving heat transfer in fused deposition modeling with graphene enhances inter filament bonding, Polym. Chem. 10(44) (2019) 5967-5978.

[100] T.N.A.T. Rahim, A.M. Abdullah, H. Md Akil, D. Mohamad, Z.A. Rajion, The improvement of mechanical and thermal properties of polyamide 12 3D printed parts by fused deposition modelling, Express Polym. Lett. 11(12) (2017) 963-982.

[101] D.P. Street, A.H. Mah, S. Patterson, D.L. Pickel, J.A. Bergman, G.E. Stein, J.M. Messman, S.M. Kilbey, Interfacial interactions in PMMA/silica nanocomposites enhance the performance of parts created by Fused Filament Fabrication, Polymer 157 (2018) 87-94.

[102] F.R. Beltrán, E. Climent-Pascual, M.U. de la Orden, J. Martínez Urreaga, Effect of solid-state polymerization on the structure and properties of mechanically recycled poly(lactic acid), Polym. Degrad. Stab. 171 (2020) 109045.

[103] G.H. Bhuvaneswari, 3 - Degradability of Polymers, in: S. Thomas, A.V. Rane, K. Kanny, A. V.K, M.G. Thomas (Eds.), Recycling of Polyurethane Foams, William Andrew Publishing, 2018, pp. 29-44.

[104] D. Thaler, N. Aliheidari, A. Ameli, Mechanical, electrical, and piezoresistivity behaviors of additively manufactured acrylonitrile butadiene styrene/carbon nanotube nanocomposites, Smart Mater. Struct. 28(8) (2019) 084004.

[105] C. Aumnate, A. Pongwisuthiruchte, P. Pattananuwat, P. Potiyaraj, Fabrication of ABS/Graphene oxide composite filament for fused filament fabrication (FFF) 3D printing, Adv. Mater. Sci. Eng. 2018 (2018) 2830437.

[106] J.A. Travieso-Rodriguez, M.D. Zandi, R. Jerez-Mesa, J. Lluma-Fuentes, Fatigue behavior of PLA-wood composite manufactured by fused filament fabrication, J. Mater. Res. Technol. 9(4) (2020) 8507-8516.

[107] J.J. Fallon, S.H. McKnight, M.J. Bortner, Highly loaded fiber filled polymers for material extrusion: A review of current understanding, Addit. Manuf. 30 (2019) 100810.

[108] H. Khoshnevis, T.Q. Tran, S.M. Mint, A. Zadhoush, H.M. Duong, M. Youssefi, Effect of alignment and packing density on the stress relaxation process of carbon nanotube fibers

spun from floating catalyst chemical vapor deposition method, Colloids Surf. A Physicochem. Eng. Asp. 558 (2018) 570-578.

[109] H.L. Tekinalp, V. Kunc, G.M. Velez-Garcia, C.E. Duty, L.J. Love, A.K. Naskar, C.A. Blue, S. Ozcan, Highly oriented carbon fiber–polymer composites via additive manufacturing, Compos. Sci. Technol. 105 (2014) 144-150.

[110] N.A. Nguyen, C.C. Bowland, A.K. Naskar, A general method to improve 3D-printability and inter-layer adhesion in lignin-based composites, Appl. Mater. Today 12 (2018) 138-152.

[111] X. Zhang, L. Chen, C. Kowalski, T. Mulholland, T.A. Osswald, Nozzle flow behavior of aluminum/polycarbonate composites in the material extrusion printing process, J. Appl. Polym. Sci. 136(12) (2019) 47252.

[112] T. Beran, T. Mulholland, F. Henning, N. Rudolph, T.A. Osswald, Nozzle clogging factors during fused filament fabrication of spherical particle filled polymers, Addit. Manuf. 23 (2018) 206-214.

[113] M.E. Mackay, The importance of rheological behavior in the additive manufacturing technique material extrusion, J. Rheol. 62(6) (2018) 1549-1561.

[114] D.D. Phan, Z.R. Swain, M.E. Mackay, Rheological and heat transfer effects in fused filament fabrication, J. Rheol. 62(5) (2018) 1097-1107.

[115] A. Das, E.L. Gilmer, S. Biria, M.J. Bortner, Importance of Polymer Rheology on Material Extrusion Additive Manufacturing: Correlating Process Physics to Print Properties, ACS Appl. Polym. Mater. 3(3) (2021) 1218-1249.

[116] D. Jiang, D.E. Smith, Anisotropic mechanical properties of oriented carbon fiber filled polymer composites produced with fused filament fabrication, Addit. Manuf. 18 (2017) 84-94.

[117] S. Dul, L. Fambri, A. Pegoretti, Filaments Production and Fused Deposition Modelling of ABS/Carbon Nanotubes Composites, Nanomaterials 8(1) (2018) 49.

[118] F. Ning, W. Cong, J. Qiu, J. Wei, S. Wang, Additive manufacturing of carbon fiber reinforced thermoplastic composites using fused deposition modeling, Compos. Part B Eng. 80 (2015) 369-378.

[119] M.L. Shofner, K. Lozano, F.J. Rodríguez-Macías, E.V. Barrera, Nanofiber-reinforced polymers prepared by fused deposition modeling, J. Appl. Polym. Sci. 89(11) (2003) 3081-3090.

[120] L. Yang, S. Li, X. Zhou, J. Liu, Y. Li, M. Yang, Q. Yuan, W. Zhang, Effects of carbon nanotube on the thermal, mechanical, and electrical properties of PLA/CNT printed parts in the FDM process, Synth. Met. 253 (2019) 122-130.

[121] G.-T. Pan, S. Chong, H.-J. Tsai, W.-H. Lu, T.C.K. Yang, The Effects of Iron, Silicon, Chromium, and Aluminum Additions on the Physical and Mechanical Properties of Recycled 3D Printing Filaments, Adv. in Polym. Technol. 37(4) (2018) 1176-1184.

[122] M. Herrero, F. Peng, K.C. Núñez Carrero, J.C. Merino, B.D. Vogt, Renewable Nanocomposites for Additive Manufacturing Using Fused Filament Fabrication, ACS Sustain. Chem. Eng. 6(9) (2018) 12393-12402.

[123] P. Parnian, A. D'Amore, Fabrication of High-Performance CNT Reinforced Polymer Composite for Additive Manufacturing by Phase Inversion Technique, Polymers 13(22) (2021) 4007.

[124] T.Q. Tran, Z. Fan, P. Liu, H.M. Duong, Advanced morphology-controlled manufacturing of carbon nanotube fibers, thin films and aerogels from aerogel technique, Asia Pacific Confederation of Chemical Engineering Congress 2015: APCChE 2015, incorporating CHEMECA 2015, Engineers Australia, 2015, p. 2444.

[125] C. Yang, X. Tian, T. Liu, Y. Cao, D. Li, 3D printing for continuous fiber reinforced thermoplastic composites: mechanism and performance, Rapid Prototyp. J. 23(1) (2017) 209-215.

[126] R. Matsuzaki, M. Ueda, M. Namiki, T.-K. Jeong, H. Asahara, K. Horiguchi, T. Nakamura, A. Todoroki, Y. Hirano, Three-dimensional printing of continuous-fiber composites by in-nozzle impregnation, Sci. Rep. 6 (2016) 23058-23058.

[127] M. Heidari-Rarani, M. Rafiee-Afarani, A.M. Zahedi, Mechanical characterization of FDM 3D printing of continuous carbon fiber reinforced PLA composites, Compos. Part B Eng. 175 (2019) 107147.

[128] N. Li, Y. Li, S. Liu, Rapid prototyping of continuous carbon fiber reinforced polylactic acid composites by 3D printing, J. Mater. Process. Technol. 238 (2016) 218-225.

[129] B. Akhoundi, A.H. Behravesh, A.B. Saed, An innovative design approach in three-dimensional printing of continuous fiber reinforced thermoplastic composites via fused deposition modeling process: In-melt simultaneous impregnation, Proc. Inst. Mech. Eng. Part B J. Eng. Manuf. 234 (2020) 243-259.

[130] X. Tian, T. Liu, Q. Wang, A. Dilmurat, D. Li, G. Ziegmann, Recycling and remanufacturing of 3D printed continuous carbon fiber reinforced PLA composites, J. Clean. Prod. 142 (2017) 1609-1618.

[131] A.N. Dickson, J.N. Barry, K.A. McDonnell, D.P. Dowling, Fabrication of continuous carbon, glass and Kevlar fibre reinforced polymer composites using additive manufacturing, Addit. Manuf. 16 (2017) 146-152.

[132] G.W. Melenka, B.K.O. Cheung, J.S. Schofield, M.R. Dawson, J.P. Carey, Evaluation and prediction of the tensile properties of continuous fiber-reinforced 3D printed structures, Compos. Struct. 153 (2016) 866-875.

[133] Y. Peng, Y. Wu, K. Wang, G. Gao, S. Ahzi, Synergistic reinforcement of polyamide-based composites by combination of short and continuous carbon fibers via fused filament fabrication, Compos. Struct. 207 (2019) 232-239.

[134] J. Naranjo-Lozada, H. Ahuett-Garza, P. Orta-Castañón, W.M.H. Verbeeten, D. Sáiz-González, Tensile properties and failure behavior of chopped and continuous carbon fiber composites produced by additive manufacturing, Addit. Manuf. 26 (2019) 227-241.

[135] K. Agarwal, S.K. Kuchipudi, B. Girard, M. Houser, Mechanical properties of fiber reinforced polymer composites: A comparative study of conventional and additive manufacturing methods, J. Compos. Mater. 52(23) (2018) 3173-3181.

[136] F.V.D. Klift, Y. Koga, A. Todoroki, M. Ueda, Y. Hirano, R. Matsuzaki, 3D Printing of Continuous Carbon Fibre Reinforced Thermo-Plastic (CFRTP) Tensile Test Specimens, Open J. Compos. Mater. 6 (2016) 18-27.

[137] L.G. Blok, M.L. Longana, H. Yu, B.K.S. Woods, An investigation into 3D printing of fibre reinforced thermoplastic composites, Addit. Manuf. 22 (2018) 176-186.

[138] G.D. Goh, V. Dikshit, A.P. Nagalingam, G.L. Goh, S. Agarwala, S.L. Sing, J. Wei, W.Y. Yeong, Characterization of mechanical properties and fracture mode of additively manufactured carbon fiber and glass fiber reinforced thermoplastics, Mater. Des. 137 (2018) 79-89.

[139] M. Araya-Calvo, I. López-Gómez, N. Chamberlain-Simon, J.L. León-Salazar, T. Guillén-Girón, J.S. Corrales-Cordero, O. Sánchez-Brenes, Evaluation of compressive and flexural properties of continuous fiber fabrication additive manufacturing technology, Addit. Manuf. 22 (2018) 157-164.

[140] J. Justo, L. Távara, L. García-Guzmán, F. París, Characterization of 3D printed long fibre reinforced composites, Compos. Struct. 185 (2018) 537-548.

[141] S. Terekhina, S. Egorov, T. Tarasova, I. Skornyakov, L. Guillaumat, M.L. Hattali, In-nozzle impregnation of continuous textile flax fiber/polyamide 6 composite during FFF process, Compos. Part A Appl. Sci. Manuf. 153 (2022) 106725.

[142] S.K. Kim, D.O. Kazmer, A.R. Colon, T.J. Coogan, A.M. Peterson, Non-Newtonian modeling of contact pressure in fused filament fabrication, J. Rheol. 65(1) (2021) 27-42.

[143] T.J. Coogan, D.O. Kazmer, Modeling of interlayer contact and contact pressure during fused filament fabrication, J. Rheol. 63(4) (2019) 655-672.

[144] S.S. Luke, D. Soares, J.V. Marshall, J. Sheddden, Ö. Keleş, Effect of fiber content and fiber orientation on mechanical behavior of fused filament fabricated continuous-glass-fiber-reinforced nylon, Rapid Prototyp. J. 27(7) (2021) 1346-1354.

[145] R.R. Fernandes, A.Y. Tamijani, M. Al-Haik, Mechanical characterization of additively manufactured fiber-reinforced composites, Aerosp. Sci. Technol. 113 (2021) 106653.

[146] I. Papa, A.T. Silvestri, M.R. Ricciardi, V. Lopresto, A. Squillace, Effect of Fibre Orientation on Novel Continuous 3D-Printed Fibre-Reinforced Composites, Polymers 13(15) (2021) 2524.

[147] G. Li, J. Zhao, J. Jiang, H. Jiang, W. Wu, M. Tang, Ultrasonic strengthening improves tensile mechanical performance of fused deposition modeling 3D printing, Int. J. Adv. Manuf. Technol. 96(5) (2018) 2747-2755.

[148] L. Chen, X. Zhang, Modification the surface quality and mechanical properties by laser polishing of Al/PLA part manufactured by fused deposition modeling, Appl. Surf. Sci. 492 (2019) 765-775.

[149] W. Jo, O.C. Kwon, M.W. Moon, Investigation of influence of heat treatment on mechanical strength of FDM printed 3D objects, Rapid Prototyp. J. 24(3) (2018) 637-644.

[150] S. Bhandari, R.A. Lopez-Anido, D.J. Gardner, Enhancing the interlayer tensile strength of 3D printed short carbon fiber reinforced PETG and PLA composites via annealing, Addit. Manuf. 30 (2019) 100922.

[151] A. Das, A.E.C. Marnot, J.J. Fallon, S.M. Martin, E.G. Joseph, M.J. Bortner, Material Extrusion-Based Additive Manufacturing with Blends of Polypropylene and Hydrocarbon Resins, ACS Appl. Polym. Mater. 2(2) (2020) 911-921.

[152] S. Gantenbein, K. Masania, W. Woigk, J.P.W. Sesseg, T.A. Tervoort, A.R. Studart, Three-dimensional printing of hierarchical liquid-crystal-polymer structures, Nature 561(7722) (2018) 226-230.

[153] Y. Wang, Z. Liu, H. Gu, C. Cui, J. Hao, Improved mechanical properties of 3D-printed SiC/PLA composite parts by microwave heating, J. Mater. Res. 34(20) (2019) 3412-3419.

[154] A. Todoroki, T. Oasada, M. Ueda, R. Matsuzaki, Y. Hirano, Reinforcing in the lay-up direction with self-heating for carbon fiber composites fabricated using a fused filament fabrication 3D printer, Compos. Struct. 266 (2021) 113815.

[155] N.P. Levenhagen, M.D. Dadmun, Reactive Processing in Extrusion-Based 3D Printing to Improve Isotropy and Mechanical Properties, Macromolecules 52(17) (2019) 6495-6501.

[156] P. Han, A. Tofangchi, A. Deshpande, S. Zhang, K. Hsu, An approach to improve interface healing in FFF-3D printed Ultem 1010 using laser pre-deposition heating, Procedia Manuf. 34 (2019) 672-677.

[157] J. Du, Z. Wei, X. Wang, J. Wang, Z. Chen, An improved fused deposition modeling process for forming large-size thin-walled parts, J. Mater. Process. Technol. 234 (2016) 332-341.

[158] M.R.A. S. N. A. Majid, F. R. Ramli, S. Maidin, T. C. Fai, M. N. Sudin, Influence of Integrated Pressing during Fused Filament Fabrication on Tensile Strength and Porosity, J. Mech. Eng. 2 (2017) 185-195.

[159] Ö. Keleş, H. Anderson Eric, J. Huynh, Mechanical reliability of short carbon fiber reinforced ABS produced via vibration assisted fused deposition modeling, Rapid Prototyp. J. 24(9) (2018) 1572-1578.

[160] S. Jiang, Y. Siyajeu, Y. Shi, S. Zhu, H. Li, Improving the forming quality of fused filament fabrication parts by applied vibration, Rapid Prototyp. J. 26(1) (2020) 202-212.

[161] A. Tofangchi, P. Han, J. Izquierdo, A. Iyengar, K. Hsu, Effect of Ultrasonic Vibration on Interlayer Adhesion in Fused Filament Fabrication 3D Printed ABS, Polymers 11(2) (2019) 315.

[162] S.N.H. Mazlan, M.R. Alkahari, N.A. Maidin, F. Ramli, M.N. Sudin, L.G. Dong, I.S. Mohamad, Influence of inert gas assisted 3 D printing machine on the surface roughness and strength of printed component, Proceedings of Mechanical Engineering Research Day 2018, pp. 154-155.

[163] D. Ravoori, H. Prajapati, V. Talluru, A. Adnan, A. Jain, Nozzle-integrated pre-deposition and post-deposition heating of previously deposited layers in polymer extrusion based additive manufacturing, Addit. Manuf. 28 (2019) 719-726.